

Exchange-dominated origin of spin-wave nonreciprocity in planar magnetic multilayers

Claudia Negrete,¹ Attila Kákay,² and Jorge A. Otálora^{1, a)}

¹⁾Departamento de Física, Universidad Católica del Norte, Avenida Angamos 0610, Antofagasta, Chile

²⁾Helmholtz-Zentrum Dresden - Rossendorf, Institute of Ion Beam Physics and Materials Research, Bautzner Landstr. 400, 01328 Dresden, Germany

(Dated: January 29, 2026)

Spin-wave nonreciprocity, manifested as a frequency difference between counterpropagating modes, underpins many proposed magnonic devices. While this effect is commonly attributed to dipolar interactions or interfacial chirality, the microscopic origin of nonreciprocal dispersion in magnetic multilayers remains under debate. Here, we analyze nonreciprocal spin-wave dispersion in planar multilayer heterostructures without Dzyaloshinskii-Moriya interaction. Using a frequency-shift dynamic matrix and an interaction-resolved dynamic energy-density formalism, we show that the frequency asymmetry cannot generally be ascribed to dipolar effects alone. Instead, once counterpropagating modes differ in their geometric structure along the thickness, interlayer exchange dominates the frequency shift. Applied to representative multilayer systems, we find that the interlayer exchange contribution exceeds dipolar and intralayer exchange effects by up to two to three orders of magnitude over a broad wave-vector range. Our results establish interlayer exchange as the primary mechanism controlling nonreciprocal dispersion in multilayer magnonic systems and provide a quantitative framework for engineering large frequency shifts in nonreciprocal magnonic devices.

I. INTRODUCTION

In the context of spin waves (SWs) - the collective eigenexcitations of an arrangement of magnetic moments - nonreciprocity is usually understood as the frequency difference between counterpropagating SWs with the same wave-vector magnitude k . In such cases, the dispersion relation (i.e., the SW oscillation frequency ω as a function of the wave vector \mathbf{k}) is said to be nonreciprocal, $\omega(\mathbf{k}) \neq \omega(-\mathbf{k})$, leading to a finite frequency difference $\Delta\omega(\mathbf{k}) = \omega(\mathbf{k}) - \omega(-\mathbf{k}) \neq 0$. Identifying and controlling the conditions that give rise to this nonreciprocal effect has been the subject of extensive theoretical and experimental efforts^{1–5}. This interest is largely motivated by the fact that nonreciprocity constitutes a fundamental mechanism for enhancing the capabilities of sensing, processing, transmission, and buffering of information encoded in the oscillatory properties of SWs in magnetic systems.⁶ Examples of applications include magnetic circulators and isolators for directional signal control^{7–9}, the suppression of backscattering noise in SW logic gates and magnetic computing circuits^{10–12}, nonreciprocal passive filters that improve signal quality by eliminating interference in a specific propagation direction in wireless networks^{13,14}, and spin-wave-based diodes that enable unidirectional wave transmission, which is essential for controlled signal routing in magnetic circuits for wave-based computing^{15,16}.

Over the past decade, significant efforts have been devoted to engineering dispersion nonreciprocity, including curving magnetic membranes^{17–20}, grading the saturation magnetization in planar magnetic films^{21,22}, stacking membranes composed of different magnetic materials^{15,23}, and piling up magnetic membranes exhibiting intrinsic spin-orbit interactions,

such as the Dzyaloshinskii-Moriya interaction (DMI)^{24–26}, among others. Despite this progress, a striking asymmetry exists in how different magnetic interactions are treated in the interpretation of nonreciprocal dispersion. In most studies, dipolar interactions-and, where present, DMI are identified as the primary origin of frequency nonreciprocity, while exchange and anisotropy interactions are assumed to play at most a secondary or indirect role^{27,28}. This interpretation is often motivated by the observation that only dipolar or chiral interactions generate explicitly wavevector-odd contributions to the dynamic matrix. However, such reasoning implicitly assumes that counterpropagating SW modes are geometrically equivalent, an assumption that does not generally hold in multilayer or vertically inhomogeneous systems.

Recently, symmetry-based approaches using quantities such as the toroidal moment have been proposed to predict dispersion nonreciprocity based solely on the equilibrium magnetic configuration and the propagation direction^{29,30}. While powerful, these approaches do not explicitly resolve how individual interactions contribute to the frequency shift once the full dynamical mode structure is taken into account. In particular, the role of exchange interactions in nonreciprocal systems - especially interlayer exchange in multilayer stacks - remains insufficiently understood.

In this work, we address this gap by analyzing the full interaction-resolved origin of spin-wave frequency shifts in planar heterostructured multilayer magnetic systems without DMI. Using a dynamic-matrix formalism for Damon-Eshbach spin waves, we demonstrate that exchange interactions can dominate the nonreciprocal frequency shift whenever counterpropagating modes differ in their geometric structure along the thickness. By introducing a frequency-shift dynamic matrix and an interaction-resolved dynamic energy density, we show that the observed nonreciprocity results from an exchange-dominated energetic imbalance driven by dipolar-induced mode asymmetry. This provides a unified physical

^{a)}Corresponding author: jorge.otalora@ucn.cl

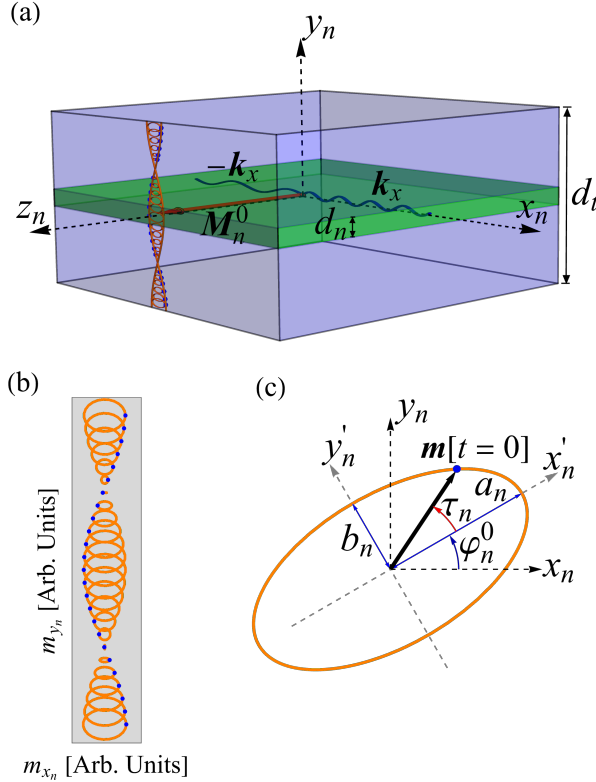


Figure 1. (a) Illustration of multilayer in a homogeneous magnetization state with a total thickness d_t . (b) Spin-wave orbits of the third excitation mode. (c) The time trajectory of the magnetization, which describes elliptical orbits due to precession, is illustrated.

mechanism that reconciles seemingly dipolar-driven dispersion asymmetries with an underlying exchange origin, and applies broadly to experimentally relevant multilayer systems.

II. THEORETICAL MODEL

The system under consideration is described within the continuum micromagnetic framework using the dynamic matrix method (DMM). We consider a planar heterostructure composed of a multilayer stack of N magnetically coupled sublayers. The magnetization dynamics of each sublayer is governed by the Landau-Lifshitz (LL) equation, resulting in a system of N coupled LL equations. The n 'th sublayer is characterized by a magnetization vector \mathbf{M}_n , an exchange length $l_{\text{ex},n}$, an exchange stiffness constant A_n and a saturation magnetization $M_{s,n}$.

Figure 1(a) illustrates the geometry of the system, which has a total thickness d_t . The n th sublayer has thickness d_n and lies in the $y_n z_n$ plane. Counterpropagating spin waves propagate along the \hat{x}_n direction with wave-vector magnitude k_x . The following assumptions are made throughout this work:

1. an external magnetic field $\mathbf{H} = H \hat{z}_n$ is applied;
2. an in-plane uniaxial anisotropy characterized by the

constant K_n^u favors magnetization alignment along the \hat{z}_n axis;

3. the isotropic exchange interaction is decomposed into an *intralayer exchange* acting within a single layer in the discretization scheme, characterized by the exchange length $l_{\text{ex},n}$,
4. and into an *interlayer exchange*, responsible for the coupling between the n th and β th sublayers, described by the integral exchange constant $J_{n,\beta}$;
5. the equilibrium magnetization state is a uniform monodomain state lying in-plane along the easy axis \hat{z}_n , given by $\mathbf{M}_n^0 = M_{s,n} \hat{z}_n$, as shown in Fig. 1(a)

We emphasize that the interlayer exchange interaction defined here should not be confused with the Ruderman-Kittel-Kasuya-Yosida (RKKY)-type interlayer exchange coupling. In the present work, the interlayer exchange refers exclusively to the conventional isotropic exchange interaction acting along the direction perpendicular to the film plane.

The LL equation governing the dynamics of the n 'th sublayer reads

$$\dot{\mathbf{M}}_n[\mathbf{r}, t] = -\mu_0 \gamma \mathbf{M}_n[\mathbf{r}, t] \times \mathbf{H}_n^e[\mathbf{r}, t], \quad (1)$$

where γ is the magnitude of the gyromagnetic ratio, $\mathbf{H}_n^e[\mathbf{r}, t]$ is the effective magnetic field acting on the n -th layer, and $\mathbf{M}_n[\mathbf{r}, t]$ is the magnetization field. The spin-wave dispersion relation and the equilibrium homogeneous state are obtained by linearizing the LL-equation around the equilibrium magnetization \mathbf{M}_n^0 . Accordingly, the magnetization and the effective field are expanded as $\mathbf{M}_n[\mathbf{r}, t] = \mathbf{M}_n^0 + \mathbf{m}_n[\mathbf{r}, t]$ and $\mathbf{H}_n^e[\mathbf{r}, t] = \mathbf{H}_n^{0e} + \mathbf{h}_n^e[\mathbf{r}, t]$, respectively. Here, \mathbf{H}_n^{0e} denotes the equilibrium effective magnetic field, while $\mathbf{m}_n[\mathbf{r}, t]$ and $\mathbf{h}_n^e[\mathbf{r}, t]$ are the dynamical perturbations. We assume plane-wave solutions of the form $\mathbf{m}_n[\mathbf{r}, t] = \int d^3\mathbf{k} e^{i(\omega t - \mathbf{k} \cdot \mathbf{r})} \tilde{\mathbf{m}}_n[\mathbf{k}]$, and $\mathbf{h}_n[\mathbf{r}, t] = \int d^3\mathbf{k} e^{i(\omega t - \mathbf{k} \cdot \mathbf{r})} \tilde{\mathbf{h}}_n[\mathbf{k}]$, where $\tilde{\mathbf{m}}_n[\mathbf{k}]$ and $\tilde{\mathbf{h}}_n[\mathbf{k}]$ are the dynamic magnetization and magnetic field in wave vector \mathbf{k} space, respectively, and ω is the angular resonance frequency of the spin waves.

Linearization of the LL equation around the equilibrium state \mathbf{M}_n^0 yields the eigenvalue problem

$$\omega \tilde{\mathbf{m}}[\mathbf{k}] = \mathbb{N}[\mathbf{k}] \tilde{\mathbf{m}}[\mathbf{k}], \quad (2)$$

where \mathbb{N} is the dynamic matrix of dimension $2N \times 2N$, with N the number of sublayers, ω is the eigenvalue, and $\tilde{\mathbf{m}}[\mathbf{k}]$ is the corresponding eigenvector with transpose $\tilde{\mathbf{m}}[\mathbf{k}]^T = \{\tilde{m}_{X_1}[\mathbf{k}], \dots, \tilde{m}_{X_N}[\mathbf{k}], \tilde{m}_{Y_1}[\mathbf{k}], \dots, \tilde{m}_{Y_N}[\mathbf{k}]\}$. A representative second-order spin-wave mode profile across the multilayer thickness is shown in Fig. 1(b), where the blue dot point indicates the dynamic magnetization at zero time ($\mathbf{m}_n[t = 0]$). The SW orbit at the n -th layer is also illustrated in Fig. 1(c), where the geometrical parameter as large(smaller) semiaxis $a_n(b_n)$, tilting angle φ_n^0 and zero-time phase (also named here as phase) τ_n are shown as well.

Explicit expressions for the dynamic matrix \mathbb{N} in multilayer systems have been reported previously^{22,23}. In the following, we therefore focus on the specific matrix components relevant to Damon-Eschbach (DE) spin waves, for which the wavevector $\mathbf{k} = k_x \hat{x}$ is perpendicular to the equilibrium magnetization $\mathbf{M}_0 = M_{s_n} \hat{z}$ (see Fig. 1(a)).

The total dynamic matrix can be expressed as the sum of contributions from dipolar (dip), intralayer exchange (ex), interlayer exchange (int), uniaxial anisotropy (U), and Zeeman (Ze) interactions, $\mathbb{N} = \mathbb{N}^{\text{dip}} + \mathbb{N}^{\text{ex}} + \mathbb{N}^{\text{int}} + \mathbb{N}^{\text{U}} + \mathbb{N}^{\text{Ze}}$. Each contribution has the block structure

$$\mathbb{N}^\sigma = \begin{pmatrix} \mathbb{N}_{xx}^\sigma & \mathbb{N}_{xy}^\sigma \\ \mathbb{N}_{yx}^\sigma & \mathbb{N}_{yy}^\sigma \end{pmatrix} \quad (3)$$

with σ running on the labels $\{\text{dip, int, ex, U, Ze}\}$. The submatrices \mathbb{N}_{ij}^σ are defined as

$$\mathbb{N}_{ij}^\sigma = \begin{pmatrix} N_{11}^{ij,\sigma} & N_{12}^{ij,\sigma} & \dots & N_{1N}^{ij,\sigma} \\ N_{21}^{ij,\sigma} & N_{22}^{ij,\sigma} & \dots & N_{2N}^{ij,\sigma} \\ \vdots & \vdots & \ddots & \vdots \\ N_{N1}^{ij,\sigma} & N_{N2}^{ij,\sigma} & \dots & N_{NN}^{ij,\sigma} \end{pmatrix}, \quad (4)$$

where i and j run on the labels $\{x, y\}$, and $N_{np}^{ij,\sigma}$ with $n, p = 1, 2, \dots, N$ are the dynamic matrix entries of \mathbb{N}_{ij}^σ . Solving Eq. (2) yields both the dispersion relation $\omega[\mathbf{k}]$ and the spin-wave eigenvectors $\tilde{\mathbf{m}}[\mathbf{k}]$.

The dynamic matrix entries of the individual interactions are shown in the supplementary material. However, for the completeness of the manuscript, are also summarized in the following. For the dipolar, intralayer exchange, uniaxial anisotropy, and Zeeman interactions, the dynamic matrix entries take the form

$$N_{np}^{xx,\text{a}} = -i \omega_{s_n} A_{np}^{xy,\text{a}}, \quad (5)$$

$$N_{np}^{xy,\text{a}} = -i \omega_{s_n} A_{np}^{yy,\text{a}}, \quad (6)$$

$$N_{np}^{yx,\text{a}} = i \omega_{s_n} A_{np}^{xx,\text{a}}, \quad (7)$$

$$N_{np}^{yy,\text{a}} = i \omega_{s_n} A_{np}^{xy,\text{a}}, \quad (8)$$

where $A_{np}^{ij,\text{a}}$ with i, j and a running on the labels $\{x, y\}$ and $\{\text{dip, ex, U, Ze}\}$, are the dynamic factors that relate the dynamic magnetization in the p -th layer $\tilde{\mathbf{m}}_p[\mathbf{k}] = \tilde{m}_{x_p} \hat{x} + \tilde{m}_{y_p} \hat{y}$ to the dynamic magnetic field in the n -th layer $\tilde{\mathbf{h}}_{np}^{\text{a}}[\mathbf{k}]$. More explicitly

$$\tilde{\mathbf{h}}_{np}^{\text{a}}[\mathbf{k}] = \begin{pmatrix} \tilde{h}_{x_np}^{\text{a}}[\mathbf{k}] \\ \tilde{h}_{y_np}^{\text{a}}[\mathbf{k}] \end{pmatrix} = \begin{pmatrix} A_{np}^{xx,\text{a}} & A_{np}^{xy,\text{a}} \\ A_{np}^{yx,\text{a}} & A_{np}^{yy,\text{a}} \end{pmatrix} \begin{pmatrix} \tilde{m}_{x_p}[\mathbf{k}] \\ \tilde{m}_{y_p}[\mathbf{k}] \end{pmatrix}, \quad (9)$$

where the explicit expressions of $A_{np}^{ij,\text{a}}$ are given in supplementary material. The dynamic matrix entries for the interlayer exchange interaction cannot be written in a direct relation to its corresponding dynamic factors $A_{np}^{ij,\text{int}}$ (as seen in

Eqs. (5) - (8)), and take the form

$$N_{np}^{xx,\text{int}} = 0, \quad (10)$$

$$N_{np}^{xy,\text{int}} = i \omega_{s_n} \left(\left(\frac{H_{n+1,n}^{\text{int}}}{M_{s_n}} \delta_{p,n+1} + \frac{H_{n-1,n}^{\text{int}}}{M_{s_n}} \delta_{p,n-1} \right) - \left(\frac{H_{n,n+1}^{\text{int}}}{M_{s_n}} + \frac{H_{n,n-1}^{\text{int}}}{M_{s_n}} \right) \delta_{p,n} \right), \quad (11)$$

$$N_{np}^{yx,\text{int}} = -i \omega_{s_n} \left(\left(\frac{H_{n+1,n}^{\text{int}}}{M_{s_n}} \delta_{p,n+1} + \frac{H_{n-1,n}^{\text{int}}}{M_{s_n}} \delta_{p,n-1} \right) - \left(\frac{H_{n,n+1}^{\text{int}}}{M_{s_n}} + \frac{H_{n,n-1}^{\text{int}}}{M_{s_n}} \right) \delta_{p,n} \right), \quad (12)$$

$$N_{np}^{yy,\text{int}} = 0, \quad (13)$$

where $H_{n,p}^{\text{int}}$ is the strength of the inter-exchange coupling between n 'th and p 'th layers. This field is given in the supplementary material, however we bring it here as

$$H_{n,p}^{\text{int}} = -\frac{J_{n,p}}{\mu_0 M_{s_n} d}. \quad (14)$$

For simplicity, we assume identical sublayer thicknesses $d_n = d$.

Nonreciprocity is quantified by evaluating the eigenfrequencies $\omega_{\pm} = \omega[\pm \mathbf{k}]$ and the resulting frequency shift $\Delta\omega \equiv \omega_+ - \omega_-$. A vanishing $\Delta\omega$ corresponds to reciprocal dispersion, while larger values indicate stronger nonreciprocity. Reported frequency shifts in multilayer systems typically reach 5-10 GHz (and up to 12 GHz)³¹, and are commonly attributed to dipolar interactions. This interpretation is motivated by the fact that only the dipolar matrix elements explicitly depend on the propagation direction, i.e., $N_{np}^{xx,\text{dip}}[\mathbf{k}] \neq N_{np}^{xx,\text{dip}}[-\mathbf{k}]$ and $N_{np}^{yy,\text{dip}}[\mathbf{k}] \neq N_{np}^{yy,\text{dip}}[-\mathbf{k}]$. However, as we demonstrate below, attributing nonreciprocity solely to dipolar interactions provides an incomplete physical picture. Instead, exchange interaction can play an equally important - or even dominant - role. To elucidate this mechanism, we introduce (i) a frequency-shift dynamic matrix \mathbb{W} whose eigenvalues correspond to $\Delta\omega$ and whose eigenvectors are $(\tilde{\mathbf{m}}^+, \tilde{\mathbf{m}}^-)^T$, and (ii) the dynamic energy density $\varepsilon[\mathbf{k}]$ carried by the spin wave. As shown in the following sections, the nonreciprocity of $\varepsilon[\mathbf{k}]$ provides direct insight into the interaction-resolved origin of the frequency shift.

A. Frequency Shift Dynamic Matrix (FSDM)

The frequency-shift dynamic matrix (FSDM) \mathbb{W} is an operator whose eigenvalues correspond to the frequency shift $\Delta\omega$, while its eigenvectors are the counterpropagating spin-wave oscillation modes $\tilde{\mathbf{m}}[\pm \mathbf{k}]$. The explicit form of \mathbb{W} and the derivation of its associated eigenvalue problem are presented

in the Supplementary Material. For completeness, we summarize here the key expressions. Accordingly, the eigenvalue equation defining the FSDM reads

$$\Delta\omega \tilde{\mathbf{m}}[\pm\mathbf{k}] = \mathbb{W}[\pm\mathbf{k}] \tilde{\mathbf{m}}[\pm\mathbf{k}], \quad (15)$$

which constitutes a nonlinear eigenvalue problem, since the operator \mathbb{W} depends explicitly on the spin-wave eigenmodes $\tilde{\mathbf{m}}$. Similar nonlinear eigenvalue problems are well known in other branches of physics, such as nonlinear optics and nonlinear quantum mechanics, where they are typically solved using self-consistent methods^{32,33}. Our goal is not to solve Eq. (15) explicitly, but to use the structure of \mathbb{W} , to disentangle and quantify the respective roles of dipolar, interlayer and intralayer exchange (again, only the decomposition of the isotropic exchange), and uniaxial anisotropy interactions in the frequency shift of nonreciprocal spin-wave dispersion relations.

The FSDM can be expressed as

$$\mathbb{W}^+ \equiv \mathbb{W}[+\mathbf{k}] = \mathbb{N}[+\mathbf{k}] - \tilde{\mathbb{N}}[-\mathbf{k}], \quad (16)$$

$$\mathbb{W}^- \equiv \mathbb{W}[-\mathbf{k}] = \tilde{\mathbb{N}}[+\mathbf{k}] - \mathbb{N}[-\mathbf{k}], \quad (17)$$

where $\tilde{\mathbb{N}}[\pm\mathbf{k}]$ is the transformed dynamic matrix defined by

$$\tilde{\mathbb{N}}[+\mathbf{k}] \equiv \tilde{\mathbb{O}} \mathbb{N}[-\mathbf{k}] \tilde{\mathbb{O}}^{-1}, \quad (18)$$

$$\tilde{\mathbb{N}}[-\mathbf{k}] \equiv \tilde{\mathbb{O}}^{-1} \mathbb{N}[+\mathbf{k}] \tilde{\mathbb{O}}, \quad (19)$$

and $\tilde{\mathbb{O}}$ is an operator that transforms the spin-wave mode $\tilde{\mathbf{m}}[-\mathbf{k}]$ into $\tilde{\mathbf{m}}[+\mathbf{k}]$ (i.e., $\tilde{\mathbf{m}}[+\mathbf{k}] = \tilde{\mathbb{O}}\tilde{\mathbf{m}}[-\mathbf{k}]$). This operator is defined as:

$$\tilde{\mathbb{O}} = \begin{pmatrix} \tilde{\mathbf{a}} \mathbb{R}_{11} & \tilde{\mathbf{a}} \mathbb{R}_{21} \\ \tilde{\mathbf{a}} \mathbb{R}_{12} & \tilde{\mathbf{a}} \mathbb{R}_{22} \end{pmatrix}, \quad (20)$$

where $\tilde{\mathbf{a}}$ and \mathbb{R}_{ij} with $i, j = 1, 2$, are $N \times N$ diagonal matrices. The n 'th diagonal entry of $\tilde{\mathbf{a}}$ is $\alpha_n = \|\tilde{\mathbf{m}}_n^+\| / \|\tilde{\mathbf{m}}_n^-\|$ with $\tilde{\mathbf{m}}_n^\pm = \tilde{\mathbf{m}}_n[\pm\mathbf{k}]$, and the n 'th diagonal entry of \mathbb{R}_{ij} , denoted by R_{ij}^n , is defined by the entries of the 2x2 rotational matrix

$$\mathbb{R}_n = \begin{bmatrix} R_{11}^n & R_{12}^n \\ R_{21}^n & R_{22}^n \end{bmatrix}, \quad (21)$$

that rotates the unit vectors $\hat{\mathbf{u}}_n^\pm = \tilde{\mathbf{m}}_n^\pm / \|\tilde{\mathbf{m}}_n^\pm\|$ as $\hat{\mathbf{u}}_n^+ = \mathbb{R}_n \hat{\mathbf{u}}_n^-$. The entries R_{ij}^n are in general complex, i.e., $R_{ij}^n = \text{Re}[R_{ij}^n] + \mathbf{i} \text{Im}[R_{ij}^n]$, with \mathbf{i} the imaginary complex unit.

Because \mathbb{R}_n is an unitary operator, it is sufficient to analyze the frequency shift with \mathbb{W}^+ (the analysis with \mathbb{W}^- is equivalent). Therefore, we write \mathbb{W}^+ as

$$\mathbb{W}^\pm = \begin{pmatrix} \mathbb{W}_{xx}^\pm & \mathbb{W}_{xy}^\pm \\ \mathbb{W}_{yx}^\pm & \mathbb{W}_{yy}^\pm \end{pmatrix}, \quad (22)$$

and focus in the DE configuration. In this case one can show that \mathbb{R}_{11} and \mathbb{R}_{12} are either pure real or imaginary matrices,

i.e., $(R_{11}^n)^* = \pm R_{11}^n$ and $(R_{12}^n)^* = \pm R_{12}^n$, but not simultaneously, leading to two mutually exclusive cases. The resulting expressions for the blocks \mathbb{W}_{ij}^+ ($i, j = x, y$), are

$$\begin{aligned} \mathbb{W}_{xx}^+ = \mathbf{w} & \left(\left(\mathbf{n}_{xx}^{\text{dip},+} + \mathbb{R}_{11} \left\langle \mathbf{n}_{xx}^{\text{dip},+} \right\rangle \mathbb{R}_{11}^\dagger - \mathbb{R}_{12} \left\langle \mathbf{n}_{xx}^{\text{dip},+} \right\rangle \mathbb{R}_{12}^\dagger \right) \right. \\ & + \left(\mathbb{R}_{12} \left\langle -\mathbf{n}_{xy}^{\text{dip},+} + \mathbf{n}_{xy}^{\text{int},+} + \sum_a \mathbf{n}_{xy}^{a,+} \right\rangle \mathbb{R}_{11}^\dagger \right. \\ & \left. \left. - \mathbb{R}_{11} \left\langle \mathbf{n}_{xy}^{\text{dip},+} + \mathbf{n}_{xy}^{\text{int},+} + \sum_a \mathbf{n}_{xy}^{a,+} \right\rangle \mathbb{R}_{12}^\dagger \right) + \mathbf{i} \mathbb{R}_{12} \mathbb{R}_{11}^\dagger \right), \end{aligned} \quad (23)$$

$$\begin{aligned} \mathbb{W}_{yy}^+ = \mathbf{w} & \left(\left(-\mathbf{n}_{xx}^{\text{dip},+} + \mathbb{R}_{12}^\dagger \left\langle \mathbf{n}_{xx}^{\text{dip},+} \right\rangle \mathbb{R}_{12} - \mathbb{R}_{11}^\dagger \left\langle \mathbf{n}_{xx}^{\text{dip},+} \right\rangle \mathbb{R}_{11} \right) \right. \\ & + \left(\mathbb{R}_{11}^\dagger \left\langle \mathbf{n}_{xy}^{\text{dip},+} - \mathbf{n}_{xy}^{\text{int},+} - \sum_a \mathbf{n}_{xy}^{a,+} \right\rangle \mathbb{R}_{12} \right. \\ & \left. \left. + \mathbb{R}_{12}^\dagger \left\langle \mathbf{n}_{xy}^{\text{dip},+} + \mathbf{n}_{xy}^{\text{int},+} + \sum_a \mathbf{n}_{xy}^{a,+} \right\rangle \mathbb{R}_{11} \right) - \mathbf{i} \mathbb{R}_{12} \mathbb{R}_{11}^\dagger \right), \end{aligned} \quad (24)$$

$$\begin{aligned} \mathbb{W}_{xy}^+ = \mathbf{w} & \left(- \left(\mathbb{R}_{11} \left\langle \mathbf{n}_{xx}^{\text{dip},+} \right\rangle \mathbb{R}_{12} + \mathbb{R}_{12} \left\langle \mathbf{n}_{xx}^{\text{dip},+} \right\rangle \mathbb{R}_{11} \right) \right. \\ & + \left(\mathbf{n}_{xy}^{\text{dip},+} + \mathbf{n}_{xy}^{\text{int},+} + \sum_a \mathbf{n}_{xy}^{a,+} \right) \\ & - \mathbb{R}_{11} \left\langle \mathbf{n}_{xy}^{\text{dip},+} + \mathbf{n}_{xy}^{\text{int},+} + \sum_a \mathbf{n}_{xy}^{a,+} \right\rangle \mathbb{R}_{11} \\ & \left. + \mathbb{R}_{12} \left\langle \mathbf{n}_{xy}^{\text{dip},+} - \mathbf{n}_{xy}^{\text{int},+} - \sum_a \mathbf{n}_{xy}^{a,+} \right\rangle \mathbb{R}_{12} - \mathbf{i} \mathbb{R}_{12} \mathbb{R}_{12} \right), \end{aligned} \quad (25)$$

$$\begin{aligned} \mathbb{W}_{yx}^+ = \mathbf{w} & \left(- \left(\mathbb{R}_{12}^\dagger \left\langle \mathbf{n}_{xx}^{\text{dip},+} \right\rangle \mathbb{R}_{11}^\dagger + \mathbb{R}_{11}^\dagger \left\langle \mathbf{n}_{xx}^{\text{dip},+} \right\rangle \mathbb{R}_{12}^\dagger \right) \right. \\ & + \left(\mathbf{n}_{xy}^{\text{dip},+} - \mathbf{n}_{xy}^{\text{int},+} - \sum_a \mathbf{n}_{xy}^{a,+} \right) \\ & + \mathbb{R}_{11}^\dagger \left\langle -\mathbf{n}_{xy}^{\text{dip},+} + \mathbf{n}_{xy}^{\text{int},+} + \sum_a \mathbf{n}_{xy}^{a,+} \right\rangle \mathbb{R}_{11}^\dagger \\ & \left. + \mathbb{R}_{12}^\dagger \left\langle \mathbf{n}_{xy}^{\text{dip},+} + \mathbf{n}_{xy}^{\text{int},+} + \sum_a \mathbf{n}_{xy}^{a,+} \right\rangle \mathbb{R}_{12}^\dagger - \mathbf{i} \left(\mathbb{I} - \mathbb{R}_{11}^\dagger \mathbb{R}_{11}^\dagger \right) \right), \end{aligned} \quad (26)$$

Here, $\mathbf{n}_{ij}^{a,+}$ and $\mathbf{n}_{ij}^{\text{dip},+}$ with $i, j = x, y$ are the normalized dynamic matrix blocks, defined as $\mathbb{N}_{ij}^{b,+} = \mathbf{w} \mathbf{n}_{ij}^{b,+}$, with $b \in \{\text{dip, ex, int, U, Ze}\}$; \sum_a sums with $a \in \{\text{ex, int, U, Ze}\}$, and \mathbf{w} is a $N \times N$ diagonal matrix with entries $[\mathbf{w}]_{np} = \omega_{s_n} \delta_{np}$ with $\omega_{s_n} = \gamma_0 M_{s_n}$, and $\langle \mathbf{n}_{ij}^{b,+} \rangle \equiv \tilde{\mathbf{a}}^{-1} \mathbf{n}_{ij}^{b,+} \tilde{\mathbf{a}}$.

The entries of the normalized dynamic matrices \mathbf{n}_{ij}^b are, for the relevant components

$$n_{np}^{xx,\text{dip}} = -\frac{\text{sign}[n-p]}{|\mathbf{k}|d/2} \sinh^2 \left[\frac{|\mathbf{k}|d}{2} \right] e^{-|k|d|n-p|} (1 - \delta_{np}), \quad (27)$$

$$n_{np}^{xy,\text{dip}} = \mathbf{i} \frac{1}{|\mathbf{k}|d/2} \left(-\sinh^2 \left[\frac{|\mathbf{k}|d}{2} \right] e^{|k|d|n-p|} (1 - \delta_{np}) + e^{-|k|d/2} \sinh \left[\frac{|\mathbf{k}|d}{2} \right] \delta_{np} \right), \quad (28)$$

$$n_{np}^{xy,\text{ex}} = \mathbf{i} l_{exp}^2 |\mathbf{k}|^2 \delta_{pn}, \quad (29)$$

$$n_{np}^{xy,\text{Ze}} = \mathbf{i} \frac{H}{M_{s_n}} \delta_{pn}, \quad (30)$$

$$n_{np}^{xy,\text{int}} = \mathbf{i} \left(\left(\frac{H_{n+1,n}^{\text{int}}}{M_{s_n}} \delta_{p,n+1} + \frac{H_{n-1,n}^{\text{int}}}{M_{s_n}} \delta_{p,n-1} \right) - \left(\frac{H_{n,n+1}^{\text{int}}}{M_{s_n}} + \frac{H_{n,n-1}^{\text{int}}}{M_{s_n}} \right) \delta_{p,n} \right), \quad (31)$$

$$n_{np}^{xy,\text{U}} = \mathbf{i} \frac{H_p^{\text{U}}}{M_{s_n}} \delta_{pn}, \quad (32)$$

where H_p^{U} is the uniaxial anisotropy field at the p'th layer.

The entries R_{11}^n and R_{12}^n can be determined in basis of the geometric parameters of spin wave orbit at the sublayer n: the eccentricity ϵ_n , tilting angle φ_n^0 , and phase τ_n , Fig. 1c), which define the orientation and ellipticity of these modes. Next, we show their analytical expression since they will be helpful for further discussions. Accordingly, they can be expressed as

$$\begin{aligned} \text{Re}[R_{11}^n] &= r_0^n \left(\left(\sqrt{(1 - \epsilon_n^-)^2(1 - \epsilon_n^+)^2} + 1 \right) \cos[\Delta\varphi_n^0] \cos[\Delta\tau_n] \right. \\ &\quad \left. - \left(\sqrt{1 - \epsilon_n^+)^2} + \sqrt{1 - \epsilon_n^-)^2} \right) \sin[\Delta\varphi_n^0] \sin[\Delta\tau_n] \right), \end{aligned} \quad (33)$$

$$\begin{aligned} \text{Re}[R_{12}^n] &= r_0^n \left(\left(\sqrt{1 - \epsilon_n^+)^2} + \sqrt{1 - \epsilon_n^-)^2} \right) \cos[\Delta\varphi_n^0] \sin[\Delta\tau_n] \right. \\ &\quad \left. + \left(\sqrt{(1 - \epsilon_n^+)^2(1 - \epsilon_n^-)^2} + 1 \right) \sin[\Delta\varphi_n^0] \cos[\Delta\tau_n] \right), \end{aligned} \quad (34)$$

$$\begin{aligned} \text{Im}[R_{11}^n] &= r_0^n \left(\left(1 - \sqrt{(1 - \epsilon_n^-)^2(1 - \epsilon_n^+)^2} \right) \cos[\bar{\varphi}_n^0] \sin[\Delta\tau_n] \right. \\ &\quad \left. + \left(\sqrt{1 - \epsilon_n^+)^2} - \sqrt{1 - \epsilon_n^-)^2} \right) \sin[\bar{\varphi}_n^0] \cos[\Delta\tau_n] \right), \end{aligned} \quad (35)$$

$$\begin{aligned} \text{Im}[R_{12}^n] &= r_0^n \left(\left(-\sqrt{1 - \epsilon_n^+)^2} + \sqrt{1 - \epsilon_n^-)^2} \right) \cos[\bar{\varphi}_n^0] \cos[\Delta\tau_n] \right. \\ &\quad \left. + \left(\sqrt{(1 - \epsilon_n^+)^2(1 - \epsilon_n^-)^2} - 1 \right) \sin[\bar{\varphi}_n^0] \sin[\Delta\tau_n] \right). \end{aligned} \quad (36)$$

where $r_0^n \equiv 1/\sqrt{(2 - \epsilon_n^-)^2(2 - \epsilon_n^+)^2}$, $\Delta\tau_n = \tau_n^- - \tau_n^+$ is a phase shift, $\Delta\varphi_n^0 = \varphi_n^{0-} - \varphi_n^{0+}$ is a tilting angle shift, and $\bar{\varphi}_n^0 = \varphi_n^{0+} + \varphi_n^{0-}$. Note the notation $x^\pm = x[\pm\mathbf{k}]$ apply to all SWs orbit parameters, i.e., with x running on ϵ_n , φ_n^0 and τ_n ,

which are given as

$$\epsilon_n = \sqrt{1 - \left(\frac{b_n}{a_n} \right)^2}, \quad (37)$$

$$\tan[2\varphi_n^0] = -\frac{\text{Im}[\tilde{m}_{x_n}^2] + \text{Im}[\tilde{m}_{y_n}^2]}{\text{Re}[\tilde{m}_{x_n}^2] + \text{Re}[\tilde{m}_{y_n}^2]}, \quad (38)$$

$$\tau_n = \arctan \left[\frac{\text{Re}[\tilde{m}_{y_n}]}{\text{Re}[\tilde{m}_{x_n}]} \right] - \varphi_n^0. \quad (39)$$

These relations show that the FSDM entries depend on the orbit geometry at each sublayer, and hence on how the mode profiles at $\pm\mathbf{k}$ differ along the thickness. As we will see, this dependence is crucial for understanding when the dipolar interaction alone accounts for the nonreciprocal frequency shift and when the exchange interactions, in particular interlayer exchange, become dominant.

B. Dynamic energy density

The total dynamic energy density in the multilayered magnetic system averaged over an oscillation period $T = 2\pi/\omega$ of a spin wave with wave vector \mathbf{k} can be written as

$$\varepsilon_t[\mathbf{k}, \omega] = \sum_a \varepsilon_a[\mathbf{k}, \omega], \quad (40)$$

where $\varepsilon_a[\mathbf{k}, \omega] = \sum_n \sum_p \varepsilon_{np}^a[\mathbf{k}, \omega]$ is the averaged energy contribution of the a 'th interaction to the total dynamic energy density. Here, $\varepsilon_{np}^a[\mathbf{k}]$ is defined as

$$\varepsilon_{np}^a[\mathbf{k}, \omega] = \frac{(\chi)\mu_0}{T} \int_0^T dt \mathbf{m}_n[t; \mathbf{k}, \omega] \cdot \mathbf{h}_{np}^a[t; \mathbf{k}, \omega], \quad (41)$$

where $\mathbf{a} \cdot \mathbf{b} = a_x b_x + a_y b_y$ is the usual dot product between vectors \mathbf{a} and \mathbf{b} . Eq. (41), $\varepsilon_{np}^a[\mathbf{k}, \omega]$ is the dynamic energy density at the n'th sublayer (in the same oscillation period $T = 2\pi/\omega$ and wave vector \mathbf{k}), produced by the magnetic interaction between the time-dependent dynamic magnetization at the n'th layer $\mathbf{m}_n[t; \mathbf{k}, \omega] = m_{x_n}[t; \mathbf{k}, \omega]\hat{x} + m_{y_n}[t; \mathbf{k}, \omega]\hat{y}$ and the time-dependent effective field of the a 'th interaction $\mathbf{h}_{np}^a[t; \mathbf{k}, \omega]$ produced at the n'th layer by the dynamic magnetization at the p'th layer. The parameter $\chi = -1/2$ for the dipolar interaction ($a = \text{dip}$) and $\chi = -1$ for the other interactions (a running on the labels ex, int, U and Ze).

In components, the time-dependent dynamic effective field of the a 'th interaction and dynamic magnetization are written as $\mathbf{m}_n[t; \mathbf{k}, \omega] = m_{x_n}[t; \mathbf{k}, \omega]\hat{x} + m_{y_n}[t; \mathbf{k}, \omega]\hat{y}$ and $\mathbf{h}_{np}^a[t; \mathbf{k}, \omega] = h_{x_{np}}^a[t; \mathbf{k}, \omega]\hat{x} + h_{y_{np}}^a[t; \mathbf{k}, \omega]\hat{y}$, and when evaluated at $x = 0, z = 0$, take the form³⁴:

$$m_{in}[t; \mathbf{k}, \omega] = \text{Re}[\tilde{m}_{in}[\mathbf{k}]] \cos[\omega t] - \text{Im}[\tilde{m}_{in}[\mathbf{k}]] \sin[\omega t]. \quad (42)$$

$$h_{i_{np}}^a[t; \mathbf{k}, \omega] = \text{Re}[\tilde{h}_{i_{np}}^a[\mathbf{k}]] \cos[\omega t] - \text{Im}[\tilde{h}_{i_{np}}^a[\mathbf{k}]] \sin[\omega t], \quad (43)$$

where $i = x, y$.

Considering Eqs. (42) and (43) in Eq. (41), one can obtain $\varepsilon_{np}^a[\mathbf{k}, \omega]$ for each interaction as follows:

- Dipolar interaction ($a = \text{dip}$):

$$\varepsilon_{np}^{\text{dip}}[\mathbf{k}] = -\frac{1}{2} \left(\frac{\mu_0}{2} \right) \mathcal{D}_{np}[\mathbf{k}], \quad (44)$$

where

$$\mathcal{D}_{np}[\mathbf{k}] = \frac{1}{2} \left(\langle \tilde{\mathbf{m}}_n, \tilde{\mathbf{h}}_{np}^{\text{dip}} \rangle + \langle \tilde{\mathbf{h}}_{np}^{\text{dip}}, \tilde{\mathbf{m}}_n \rangle \right) \quad (45)$$

- Interlayer exchange interaction ($a = \text{int}$):

$$\begin{aligned} \varepsilon_{np}^{\text{int}}[\mathbf{k}] = \frac{\mu_0}{2} & \left(\frac{H_{n+1,n}^{\text{int}}}{M_{s_n}} \mathcal{I}_{n+1,n} \delta_{p,n+1} \right. \\ & \left. + \frac{H_{n-1,n}^{\text{int}}}{M_{s_n}} \mathcal{I}_{n-1,n} \delta_{p,n-1} \right), \end{aligned} \quad (46)$$

where

$$\mathcal{I}_{np}[\mathbf{k}] = \frac{1}{2} (\langle \tilde{\mathbf{m}}_n, \tilde{\mathbf{m}}_p \rangle + \langle \tilde{\mathbf{m}}_p, \tilde{\mathbf{m}}_n \rangle) \quad (47)$$

- Intralayer interaction ($a = \text{ex}$):

$$\varepsilon_{np}^{\text{ex}}[\mathbf{k}] = \frac{\mu_0}{2} l_{\text{ex}_n}^2 |\mathbf{k}|^2 \mathcal{I}_{np}[\mathbf{k}] \delta_{pn}, \quad (48)$$

where $\langle \mathbf{a}, \mathbf{b} \rangle \equiv a_x^* b_x + a_y^* b_y$.

For the uniaxial anisotropy ($a = \text{U}$) and Zeeman ($a = \text{Ze}$) interactions, the dynamic fields vanish in our geometry (their dynamic demagnetizing factors are zero), so $\tilde{\mathbf{h}}_{np}^{\text{U}}[\mathbf{k}] = \tilde{\mathbf{h}}_{np}^{\text{Ze}}[\mathbf{k}] = 0$ and consequently $\varepsilon_{np}^{\text{U}}[\mathbf{k}] = \varepsilon_{np}^{\text{Ze}}[\mathbf{k}] = 0$. Thus, only dipolar, intra- and interlayer exchange interactions contribute to the dynamic energy density.

In systems with broken symmetry, the effective field and the torque on the magnetization generally differ for spin waves propagating in opposite directions. It is then natural to define the *dynamic energy-density shift* associated with interaction a as

$$\Delta \varepsilon_a[\mathbf{k}, \omega] = \varepsilon_a[+\mathbf{k}, \omega^+] - \varepsilon_a[-\mathbf{k}, \omega^-], \quad (49)$$

and the total shift as $\Delta \varepsilon_t[\mathbf{k}, \omega] = \sum_a \Delta \varepsilon_a[\mathbf{k}, \omega]$. Because the spin-wave frequency and the total dynamic energy density are closely related, one expects $\Delta \varepsilon_t$ and $\Delta \omega$ to exhibit similar trends. By evaluating $\Delta \varepsilon_a$ separately for each interaction, we obtain an energetic measure of how strongly each interaction contributes to the nonreciprocal dispersion. In particular, if $\Delta \varepsilon_{\text{int}}$ significantly exceeds $\Delta \varepsilon_{\text{dip}}$ and $\Delta \varepsilon_{\text{ex}}$, we can infer that interlayer exchange plays the dominant role in the frequency shift.

In the following sections we will use both the FSDM and the dynamic energy-density formalism to analyze the mechanisms underlying spin-wave nonreciprocity in representative multilayer systems.

III. RESULTS AND DISCUSSION

In this section we use the frequency-shift dynamic matrix (FSDM) and the dynamic energy-density formalism to identify which magnetic interactions dominate the nonreciprocal frequency shift in multilayer systems. We first clarify the special case where the nonreciprocity is purely dipolar in origin, and then show that, in general, the interlayer exchange interaction provides the leading contribution to the frequency shift, even in systems where nonreciprocity is usually attributed solely to dipolar fields. Finally, we relate these findings to the geometry of the spin-wave orbits and the rotation matrices that enter the FSDM.

A. Dipolar dominated frequency shift

It is expected that a reciprocal dispersion relation implies that $\tilde{\mathbf{m}}^+$ and $\tilde{\mathbf{m}}^-$ are heterosymmetric counterpropagating oscillation modes. However, heterosymmetric modes non necessarily implies reciprocal dispersion relation. Therefore, a convenient starting point is the case where the counterpropagating modes at a given wave vector magnitude k are *heterosymmetric* but share the same normalized profile in each sublayer,

$$\frac{\tilde{\mathbf{m}}_n^+}{\|\tilde{\mathbf{m}}_n^+\|} = \frac{\tilde{\mathbf{m}}_n^-}{\|\tilde{\mathbf{m}}_n^-\|}, \quad n = 1, \dots, N. \quad (50)$$

In terms of the orbit parameters this means that the eccentricities, tilting angles and phases coincide for $\pm \mathbf{k}$ in every sublayer ($\epsilon_n^+ = \epsilon_n^-$, $\Delta \varphi_n^0 = 0$, $\Delta \tau_n = 0$). Under these conditions the local rotation matrices reduce to the identity, $\mathbb{R}_n = \mathbb{I}^{2 \times 2}$ for all n , such that $\mathbb{R}_{11} = \mathbb{R}_{22} = \mathbb{I}^{N \times N}$ and $\mathbb{R}_{12} = \mathbb{R}_{21} = 0$. Consequently, the FSDM in Eq. (16) simplifies to

$$\mathbb{W}^+ = (\mathbb{N}^{\text{dip}}[+\mathbf{k}] - \langle \mathbb{N}^{\text{dip}}[-\mathbf{k}] \rangle) + (\mathbb{N}^{\text{int}}[+\mathbf{k}] - \langle \mathbb{N}^{\text{int}}[-\mathbf{k}] \rangle), \quad (51)$$

so that the frequency shift $\Delta \omega$ is determined by the dipolar and interlayer interactions. All other interactions appear identically in $\mathbb{N}[\mathbf{k}]$ and $\mathbb{N}[-\mathbf{k}]$ and cancel out in Eq. (51).

The frequency shift $\Delta \omega$ is determined exclusively by the nonreciprocal components of the dipolar interaction only in the identical counterpropagating modes case, $\tilde{\mathbf{m}}_n^+ = \tilde{\mathbf{m}}_n^-$, where $\tilde{\mathbf{a}} = \mathbb{I}^{N \times N}$, $\langle \mathbb{N}^{\text{int}} \rangle = \mathbb{N}^{\text{int}}$, and the FSDM acquire the form

$$\mathbb{W}^+ = \mathbb{N}^{\text{dip}}[+\mathbf{k}] - \mathbb{N}^{\text{dip}}[-\mathbf{k}], \quad (52)$$

This case coincides with the common assumption in the literature that nonreciprocity is purely dipolar in origin. However, Eqs. (52) also makes clear that this conclusion is valid only when the mode profiles are identical for $\pm \mathbf{k}$. As soon as both counterpropagating modes are different in magnitude

and norm,

$$\|\mathbf{m}_n^+\| \neq \|\mathbf{m}_n^-\| \quad (53)$$

$$\frac{\tilde{\mathbf{m}}_n^+}{\|\tilde{\mathbf{m}}_n^+\|} \neq \frac{\tilde{\mathbf{m}}_n^-}{\|\tilde{\mathbf{m}}_n^-\|} \quad (54)$$

the diagonal matrix $\tilde{\mathbf{a}}$ deviates from identity, $\tilde{\mathbf{a}} \neq \mathbb{I}$ and the full expressions in Eqs. (23)-(26) show that interlayer exchange, intralayer exchange and anisotropy terms necessarily enter the FSDM and contribute to $\Delta\omega$. In contrast, dipolar and interlayer exchange interactions only participate in the frequency shift whenever the normalized modes are identical as shown in Eq. (51).

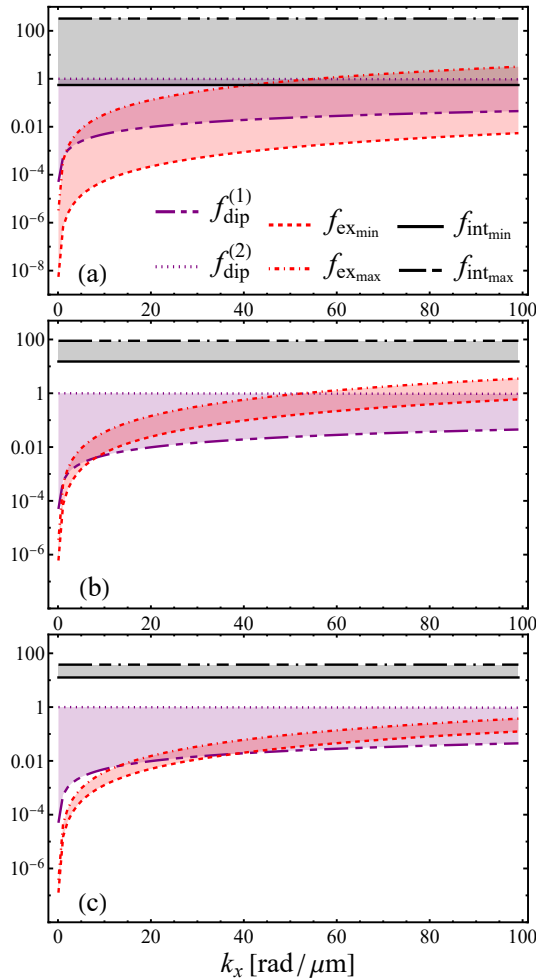


Figure 2. Dipolar strength interaction ($f_{\text{dip}}^{(1)}$ and $f_{\text{dip}}^{(2)}$), and maximum and minimum strengths of the interlayer exchange interaction ($f_{\text{int},\text{min}}$, $f_{\text{int},\text{max}}$) and intralayer exchange interaction ($f_{\text{ex},\text{min}}$, $f_{\text{ex},\text{max}}$), as a function of the wave vector k_x . (a) Geneneral multilayered film, (b) graded magnetization NiFe layer, and (c) Magnonic diode CoFeB/NiFe bilayer.

B. Interaction strengths and their role to the frequency shift

To identify the dominant interactions in the SWs frequency shift, let's first analyze the role of each interaction in the FSDM, \mathbb{W}^+ . From Eqs. (23)-(26), one can see that \mathbb{R}_{11} , \mathbb{R}_{12} and their adjoints play as the weights of the normalized dynamic matrix blocks $\mathbf{n}_{xx}^{\text{dip}}$, $\mathbf{n}_{xy}^{\text{dip}}$ and \mathbf{n}_{xy}^a with $a \in \{\text{ex, int, U and Ze}\}$. Since the norm of the entries of \mathbb{R}_{11} and \mathbb{R}_{12} are delimited between 0 and 1, thus the normalized dynamic matrices are equally weighted by them in the FSDM. Accordingly, the contribution degree of each interaction in the FSDM can be evaluated by comparing the entries among the normalized dynamic matrix blocks of the interactions. So, from Eqs. (28)-(32), we introduce the so-called “*the strength*” of each interaction as follows

$$f_{\text{dip}}^{(1)}[k] = -\frac{1}{kd/2} \sinh^2 \left[k \frac{d}{2} \right] e^{-kd}, \quad (55)$$

$$f_{\text{dip}}^{(2)}[k] = -\frac{1}{kd/2} \sinh \left[k \frac{d}{2} \right] e^{-kd/2}, \quad (56)$$

$$f_{\text{ex}_n} = l_{\text{ex}_n} |\mathbf{k}|^2, \quad (57)$$

$$f_{\text{int}_n} = \frac{H_{n+1,n}^{\text{int}}}{M_{s_n}}, \quad (58)$$

$$f_{\text{Ze}_n} = \frac{H_0}{M_{s_n}}, \quad (59)$$

$$f_{\text{U}_n} = \frac{H_n^{\text{U}}}{M_{s_n}}, \quad (60)$$

where $f_{\text{dip}}^{(1)}[k]$ and $f_{\text{dip}}^{(2)}[k]$ define the strength of the normalized dynamic dipolar blocks $\mathbf{n}_{xx}^{\text{dip}}$ and $\mathbf{n}_{xy}^{\text{dip}}$, and f_{a_n} the strength at the n 'th sublayer of the normalized dynamic a 'th block \mathbf{n}_{xy}^a with $a \in \{\text{int, ex, U, Ze}\}$.

We compare these strengths among them, so we start from a generic multilayer with its magnetic parameters spanning wide ranges along the sublayers. Hence, by adopting the notation of the X magnetic parameter ranging as $X \in [X_{\text{min}}, X_{\text{max}}]$, we have: $A_n \in [10^{-12}, 10^{-10}] \text{ J/m}$, $M_{s_n} \in [700, 1800] \times 10^3 \text{ A/m}$, $K_n^{\text{U}} \in [0, 10^6] \text{ J/m}^3$, $d = 1 \text{ nm}$, and interlayer exchange $J_{n,p} = 2A_n/d$. From these we obtain $l_{\text{ex}_n} \in [0.7, 18] \text{ nm}$, $H_{n,p}^{\text{int}} \in [0.468, 113.69] \times 10^6 \text{ A/m}$, $H_n^{\text{U}} \in [0, 0.274] \times 10^6 \text{ A/m}$ and $H \in [0, 8] \times 10^6 \text{ A/m}$. The corresponding strength ranges are then $f_{\text{int}_n} \in [0.28, 162.4]$, $f_{\text{U}_n} \in [0, 0.323]$, and $f_{\text{Ze}_n} \in [0, 1]$, while $f_{\text{ex}_n} \propto |\mathbf{k}|^2$ through l_{ex_n} .

Fig. 2(a), shows these strengths as a function of the wave vector k for the full parameter ranges, with the exception of the uniaxial anisotropy and Zeeman interactions since their maximum and minimum are constant values. Despite the wide range of parameter values, we observe that interlayer exchange interaction strength (see gray area) is mostly larger than the other interaction strengths: (i) the dipolar interaction strength (purple area) compete with the interlayer exchange strength, sharing only a reduced area between ~ 0.8 and ~ 1 for all the wave vector values, (ii) the intralayer exchange in-

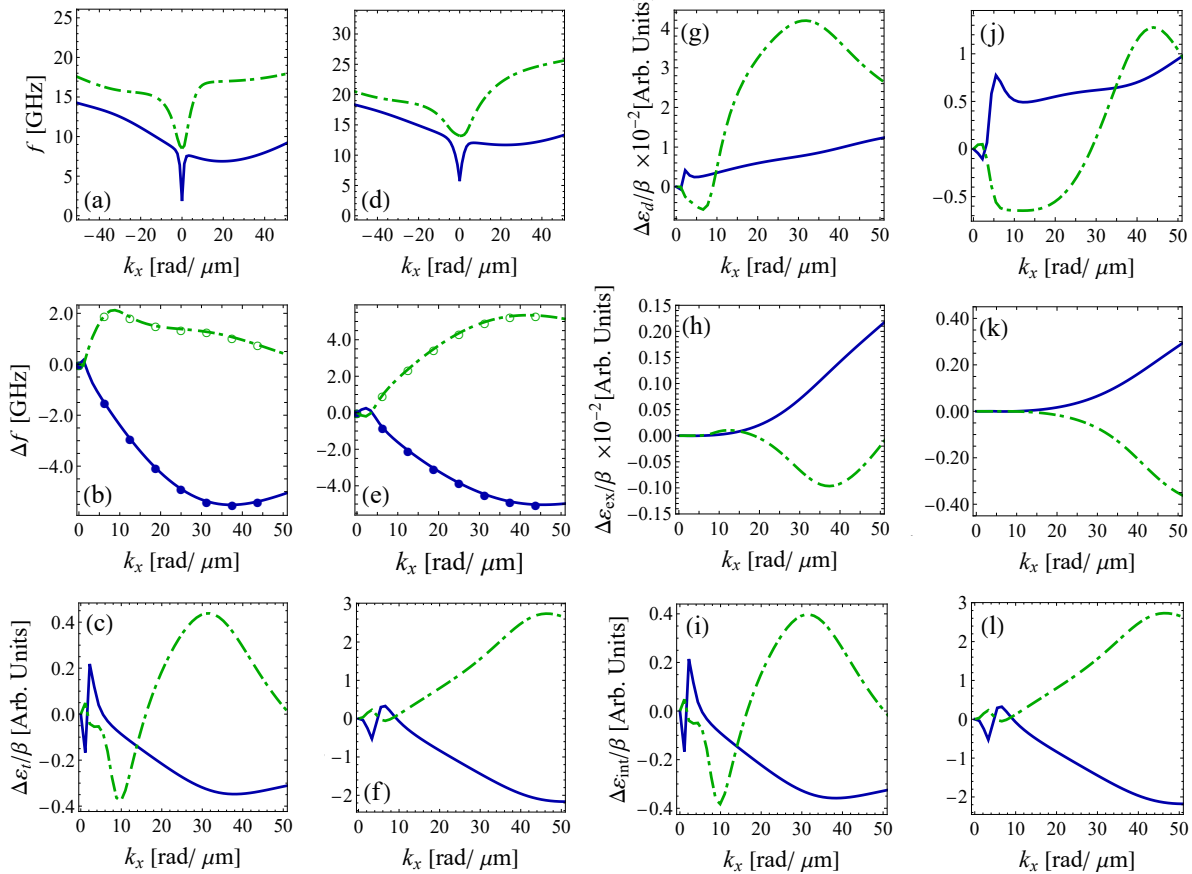


Figure 3. (a), (b) and (c) correspond to the dispersion relation f v.s k , the frequency shift $\Delta f \equiv f[k] - f[-k]$ and total energy density shift $\Delta\varepsilon \equiv \varepsilon[k] - \varepsilon[-k]$ of a graded magnetization NiFe multilayer, respectively. (d), (e) and (f) present the same quantities of a CoFeB/NiFe bilayer. (g), (h) and (i) show the energy frequency shift contribution from dipolar interaction, intra-layer interaction, inter-layer interaction of the graded magnetization NiFe multilayer, respectively, while (j), (k) and (l) show the same quantities of the CoFeB/NiFe bilayer. The blue-circle and green open circle points in (b) and (d) correspond to the frequency shift calculated with the Frequency Shift Dynamic Matrix, whereas the full blue line and dot-dashed green line correspond to the frequency shift calculated with the Dynamic Matrix. The blue and dot-dashed green curves shows the frequency, frequency shift and energy shift of the fundamental and first order spin wave modes. The planar NiFe layer has a graded magnetization saturation along the thickness whose profile changes from $M_s = 800$ kA/m to $M_s = 1600$ kA/m, a thickness $d_{t,\text{NiFe}} = 60$ nm and a stiffness constant $A_{\text{NiFe}} = 11$ pJ/m. For this system, the applied field is $\mu_0 H = 1.5$ mT along the saturation magnetization direction. The CoFeB/NiFe bilayer has a saturation magnetization, stiffness constant, thickness and uniaxial anisotropy constant as $M_s^{\text{CoFeB}} = 1270$ kA/m ($M_s^{\text{NiFe}} = 845$ kA/m), $A_{\text{CoFeB}} = 17$ pJ/m ($A_{\text{NiFe}} = 12.8$ pJ/m), $d_{t,\text{CoFeB}} = 25$ nm ($d_{t,\text{NiFe}} = 25$ nm) and $K_{\text{CoFeB}} = 0$ ($K_{\text{NiFe}} = 0$), respectively, with an applied magnetic field $\mu_0 H = 30$ mT. The parameter β is defined as $\mu_0 \pi / 2$.

teraction strength (red area) compete weakly with the intralayer strength at a wavevector range $k > 30$ rads/μm (a small portion of the gray and red areas overlaps), and (iii) the zee-mann interaction and uniaxial anisotropy strengths almost do not compete with the interlayer strength (there is almost no overleaping areas with the interlayer strength), given that the maximum strength of the both interaction ($f_{\text{Ze,max}} = 1$ and $f_{\text{U,max}} = 0.323$) is at the same order than the minimum strength value of the interlayer strength ($f_{\text{int,min}} = 0.28$).

To connect this generic analysis to realistic systems, we evaluate the strengths for two experimentally relevant cases from Ref.^{15,22}. The first system “*The magnonic diode*” (MD)¹⁵ considers a CoFeB/NiFe bilayer, where the CoFeB (NiFe) layer have a homogeneous magnetization, stiff-

ness constant, thickness and uniaxial anisotropy constant as $M_s^{\text{CoFeB}} = 1270$ kA/m ($M_s^{\text{NiFe}} = 845$ kA/m), $A_{\text{CoFeB}} = 17$ pJ/m ($A_{\text{NiFe}} = 12.8$ pJ/m), $d_{t,\text{CoFeB}} = 25$ nm ($d_{t,\text{NiFe}} = 25$ nm) and $K_{\text{CoFeB}} = 0$ ($K_{\text{NiFe}} = 0$), respectively, with an applied magnetic field $\mu_0 H = 30$ mT. The second system “*The graded magnetization layer*” (GML)²² considers a planar NiFe layer with graded saturation magnetization along the thickness whose profile changes from $M_s = 800$ kA/m to $M_s = 1600$ kA/m, a thickness $d_{t,\text{NiFe}} = 60$ nm and a stiffness constant $A_{\text{NiFe}} = 11$ pJ/m. For this system, the applied field is $\mu_0 H = 1.5$ mT along the saturation magnetization direction. Their corresponding interaction strength results in Fig 2 (b) and (c), show that in both structures the interlayer exchange strength remains the largest contribution across the

full k range. This is noteworthy because, on the one hand, in the original works the nonreciprocity was attributed primarily to dipolar effects, whereas the FSDM and strength analysis clearly indicate that interlayer exchange must play a major role, and on the other hand, they have been the basis for numerous forthcoming literature that follows a similar dipolar based explanation trend.

C. Dynamic energy density shift

Our results, which reveal the dominant contribution of the interlayer exchange strength to the entries of the FSDM, indicate that this interaction warrants a more detailed examination of its role in shaping the frequency shift of nonreciprocal dispersion relations. Motivated by this observation, we proceed with an energetic analysis that enables a separate and quantitative evaluation of the contributions of each magnetic interaction to the frequency shift in the magnonic diode (MD) and graded-magnetization layer (GML) systems. Accordingly, we evaluate the total dynamic energy density $\varepsilon_t[\mathbf{k}, \omega]$ (Eq. (40)) averaged over an oscillation period $T = 2\pi/\omega$ at a wavevector \mathbf{k} , and decompose it in the dynamic energy density contribution of the a 'th interaction $\varepsilon_a[\mathbf{k}, \omega]$, with a running on the labels {dip, ex, int}. In this analysis, the uniaxial anisotropy and Zeeman interactions contributions to the dynamic energy density are zero since the dynamic magnetic field produced by them are also zero ($\tilde{\mathbf{h}}_{np}^U[\mathbf{k}] = \tilde{\mathbf{h}}_{np}^{Ze}[\mathbf{k}] = 0$, see Eq. (9)) due to their zero dynamic factors ($A_{np}^{ij,U} = A_{np}^{ij,Ze} = 0$, see supplementary material). Now, understanding that the oscillation frequency $\omega[\mathbf{k}]$ at a wavevector \mathbf{k} of a SW mode is directly linked with the total dynamic energy density in such a sense that if $\omega[\mathbf{k}]$ increases/decreases thus $\varepsilon_t[\mathbf{k}, \omega]$ follows the same trend, we can expect a similar correlation between the dynamic energy density shift $\Delta\varepsilon_t[\mathbf{k}, \omega]$ and the frequency shift $\Delta\omega[\mathbf{k}]$. Knowing that the total dynamic energy density shift is written as the addition of the dynamic energy density shift of each contribution ($\Delta\varepsilon_t[\mathbf{k}, \omega] = \sum_a \Delta\varepsilon_a[\mathbf{k}, \omega]$ with $\Delta\varepsilon_a[\mathbf{k}, \omega] = \varepsilon_a[+\mathbf{k}, \omega^+] - \varepsilon_a[-\mathbf{k}, \omega^-]$ and a running on the interaction labels {dip, ex, int}), therefore, one can indirectly evaluate the contribution of each interaction in the frequency shift $\Delta\omega$ by evaluating separately $\Delta\varepsilon_a[\mathbf{k}, \omega]$ at each interaction (the larger is the dynamic energy shift $\Delta\varepsilon_a$ thus the larger is the influence of the a 'th interaction in the frequency shift). In this sense, one need to observe that $\Delta\varepsilon_{int}$ is much larger than $\Delta\varepsilon_{ex}$ and $\Delta\varepsilon_{dip}$ to expect that the interlayer exchange interaction contributes the most to the frequency shift of the nonreciprocal dispersion relation. This expectation is reinforced by noticing that the dynamic energy density of the a 'th interaction is proportional to the a 'th interaction strength ($\varepsilon_{dip} \propto f_{dip}^{(q)}$ with $q \in \{1, 2\}$, $\varepsilon_{ex} \propto f_{ex}$ and $\varepsilon_{int} \propto f_{int}$), hence, implying that the the dynamic energy shift of the a 'th interaction shares the same proportionality, i.e., $\Delta\varepsilon_{dip} \propto f_{dip}^{(q)}$ with $q \in \{1, 2\}$, $\Delta\varepsilon_{ex} \propto f_{ex}$ and $\Delta\varepsilon_{int} \propto f_{int}$. Hence, it is straight forward to see that if f_{int} dominates, thus $\Delta\varepsilon_{int}$ can also dominates over the other interactions, which is translated in that the interlayer exchange interaction would play a dominant role in

the frequency shift.

Fig. 3(a) and (d), reproduce the dispersion relation presented in the MD and GML references, respectively, using the eigensystem equation Eq. (2), with dynamic matrix entries shown in Eqs. (5)-(8) and Eqs. (10)-(13). The frequency shift $\Delta f = 1/(2\pi)\Delta\omega$ is calculated by the two different methods described here, continuous (fundamental SW mode) and dashed (first SW mode) lines with the dynamic matrix approach, and full and empty dots with the FSDM eigensystem Eq. 15, as seen in Figs. 3(b) and (e). This shows the expected consistency of the FSDM approach for calculating the frequency shift. The total dynamic energy density shift $\Delta\varepsilon_t/(\mu_0\pi/2)$ is calculated for the two different SW modes, as seen in figure 3(c) and (f). We observe a similar trend between the frequency shift and total dynamic energy density shift as expected. We also plotted the dynamic energy density shift separately for each interaction to check their contributing role, as see in Fig. 3 (g), (h) and (i) for the MD system and Fig. 3 (j), (k) and (l) for the GML system. One can see that $\Delta\varepsilon_{int}/(\mu_0\pi/2)$ is two(three) orders of magnitude larger than $\Delta\varepsilon_{dip}/(\mu_0\pi/2)$ ($\Delta\varepsilon_{ex}/(\mu_0\pi/2)$), therefore, showing the interlayer exchange interaction as the dominant in the frequency shift.

D. Mechanism for the frequency shift

Based on the considerations above, we propose a physical mechanism that accounts for the frequency shift observed in the nonreciprocal dispersion relation of multilayer magnetic systems. This mechanism can be viewed as a generalization of the well-known origin of frequency gaps between spin-wave modes at a given wave vector \mathbf{k} in homogeneous thin films with uniform magnetization and reciprocal dispersion relations. In such systems, the frequency splitting between modes arises from the interplay between dipolar and exchange interactions. Here, we adapt this framework to multilayer systems with nonreciprocal dispersion and show that it naturally explains our finding that the interlayer exchange interaction dominates the frequency shift.

In a homogeneous thin film, the frequency gap between spin-wave modes at the same wave vector \mathbf{k} is primarily determined by the competition between dipolar and perpendicular-to-plane exchange interactions. The dipolar interaction favors the formation of perpendicular standing spin-wave modes, characterized by increasing inhomogeneity and the appearance of nodes along the film thickness. In contrast, the exchange interaction acting perpendicular to the film plane - which, within our discretized multilayer description, corresponds to the interlayer exchange interaction - energetically penalizes such inhomogeneity. Because the interlayer exchange interaction is associated with a comparatively large strength parameter f_{int} , its contribution increases rapidly with the degree of mode nonuniformity. Consequently, differences in the thickness profiles of spin-wave modes at the same wave vector result in different interlayer exchange energies, leading to the emergence of a frequency gap.

This mechanism is clearly illustrated by the reciprocal dis-

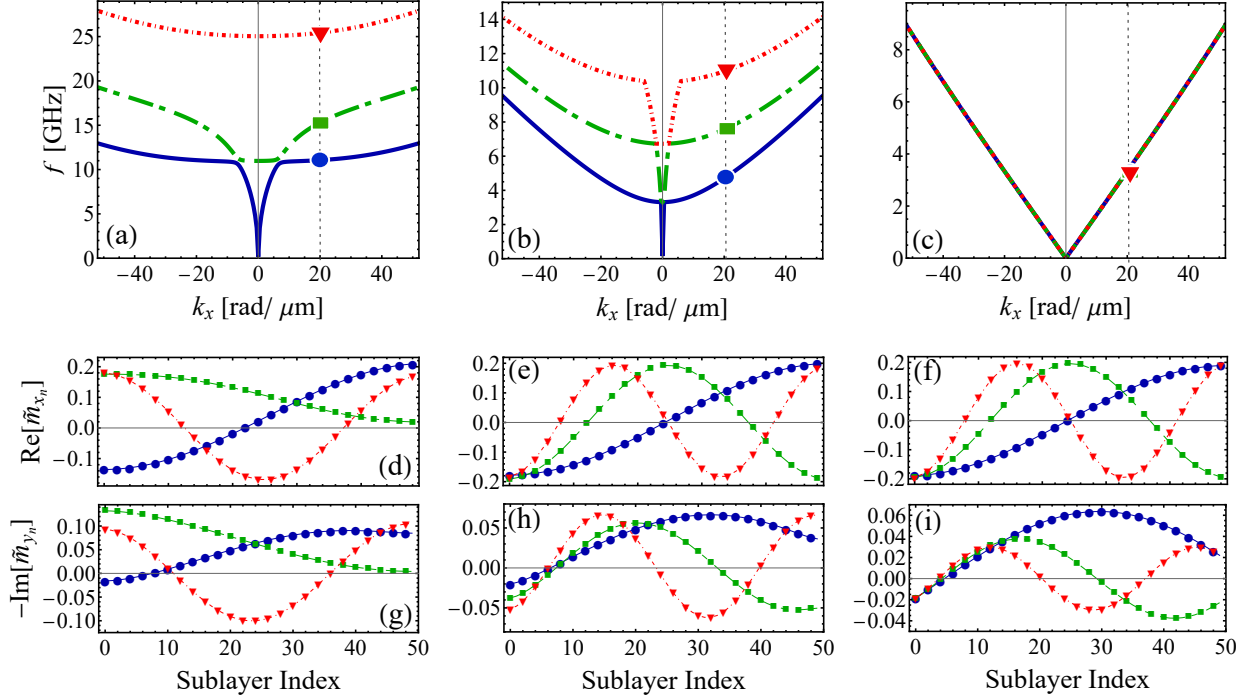


Figure 4. Dispersion relation and spin wave modes distribution at the same wavevector $k_x = 20$ rads/ μm of a homogeneous NiFe layer with in-plane homogeneous magnetization aligned along \hat{z} axis, and saturation magnetization, stiffness constant, thickness and uniaxial anisotropy constant given as $M_s^{\text{NiFe}} = 845$ kA/m, $A_{\text{NiFe}} = 12.8$ pJ/m, $t_{\text{NiFe}} = 50$ nm, and $K_{\text{NiFe}} = 0$, respectively. The first, second and third columns of plots correspond to our results at 100%, 10% and 0% of the full interlayer exchange interaction, respectively. (a)-(c) correspond to the dispersion relation, (d)-(f) and (g)-(i) correspond to the dynamic magnetization distribution along the thickness $\mathbf{m}_n[t = 0] = \text{Re}[\tilde{\mathbf{m}}_{x_n}]$ and $\mathbf{m}_n[t = \pi/2] = -\text{Im}[\tilde{\mathbf{m}}_{y_n}]$, respectively. Blue-circle, green-square and red-triangle dots correspond to the fundamental, first and second order spin wave modes.

dispersion relation of a homogeneous NiFe film calculated for 100%, 10% and 0% of the full interlayer exchange interaction strength, as shown in Fig. 4. As the interlayer exchange strength is progressively reduced, all spin-wave branches shift toward lower frequencies and the frequency gaps between modes decrease. In the limiting case of vanishing interlayer exchange, the modes become fully degenerate, exhibiting a zero frequency gap [compare Figs. 4(a) and (b) with Fig. 4(c), where all three modes collapse onto a single branch]. Notably, the fundamental spin-wave mode, which lacks nodes across the thickness (green curve in Fig. 4(b)), is present only when the interlayer exchange interaction is sufficiently strong. When the interlayer exchange is significantly weakened, only modes with nodes remain accessible, reflecting the dominance of dipolar interactions. This regime is characterized by an overall reduction in spin-wave frequencies and the degeneration of mode energies.

We now extend this mechanism to explain the frequency shift between two counterpropagating spin-wave modes $\tilde{\mathbf{m}}^\pm$ at the same wave-vector magnitude k in the Damon-Eshbach configuration. When the dipolar interaction induces different degrees of inhomogeneity along the thickness for the two counterpropagating modes, both the dipolar and exchange

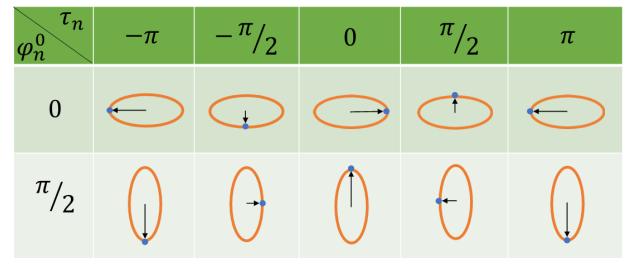


Figure 5. A single layer of NiFe with in-plane homogeneous magnetization, and saturation magnetization, stiffness constant, thickness and uniaxial anisotropy constant given as $M_s^{\text{NiFe}} = 845$ kA/m, $A_{\text{NiFe}} = 12.8$ pJ/m, $t_{\text{NiFe}} = 50$ nm, and $K_{\text{NiFe}} = 0$, respectively.

contributions to their frequencies become unequal. However, because the interlayer exchange interaction typically exceeds the dipolar interaction in strength, the resulting difference in exchange energy dominates the frequency shift. In contrast, in the special case where the mode profiles are identical, both counterpropagating modes possess the same degree of inho-

mogeneity. As a result, their interlayer (and intralayer) exchange contributions are equal, and the nonzero frequency shift arises exclusively from dipolar interactions. This analysis provides a unified physical picture in which dipolar interactions act primarily as the source of mode asymmetry, while interlayer exchange interactions convert this asymmetry into a dominant energetic and frequency imbalance, thereby governing the magnitude of the nonreciprocal frequency shift.

E. Eccentricity ϵ_n , dephase angle φ_n^0 and tilting angle τ_n , and Rotational matrices \mathbb{R}_{11} and \mathbb{R}_{12}

The $N \times N$ diagonal matrices \mathbb{R}_{11} and \mathbb{R}_{12} play a fundamental role in the FSDM \mathbb{W}^\pm , given that they weight the influence of each interaction in the frequency shift of the nonreciprocal dispersion relation, as mentioned in previous sections. As seen in Eqs. (23) - (26), these matrices weight the normalized dynamic matrix blocks $\mathbb{m}_{xx}^{\text{dip}}$, \mathbb{m}_{xy}^a at the FSDM blocks, where a runs on the labels $\{\text{dip, int, ex, U, Ze}\}$. Accordingly, these matrices deserve an analysis.

As said in previous sections, the n 'th diagonal entries of \mathbb{R}_{11} and \mathbb{R}_{12} , denoted as R_{11}^n and R_{12}^n respectively, correspond to the first line entries of the n 'th unitary 2×2 rotational matrix \mathbb{R}_n as seen in Eq. (21), with $n = 1, 2, \dots, N$. Since \mathbb{R}_n transforms $\tilde{\mathbf{m}}_n^- / \|\tilde{\mathbf{m}}_n^-\|$ into $\tilde{\mathbf{m}}_n^+ / \|\tilde{\mathbf{m}}_n^+\|$, $\tilde{\mathbf{m}}_n^\pm$ is related with the dynamic magnetization $\mathbf{m}_n[t; \pm \mathbf{k}, \omega]$ via Eqs. (42), and the dynamic magnetization can be written in terms of the orbits parameters, thus, R_{11}^n and R_{12}^n can be also written in terms of the Eccentricity ϵ_n , tilting angle φ_n^0 and phase shift τ_n , as seen in Eqs. (33)-(36). Therefore, in the following we analyze the behaviour of R_{11}^n and R_{12}^n as function of the wavevector for all sublayers, correlating them with the orbit parameters. To this end, let's analyze the orbit parameters of the fundamental SW mode as function of the wavevector for a NiFe homogeneous film with homogeneous magnetization, and the nonreciprocal MD and the GML systems, to analyze later the matrices \mathbb{R}_{11}^n , and \mathbb{R}_{12}^n .

The eccentricity ϵ_n , phase shift τ_n and tilting angle φ_n^0 are calculated by obtaining the eigenmodes $\tilde{\mathbf{m}}$ at a given wavevector \mathbf{k} , thus replacing them in Eqs. (37)-(39). Fig. 6 shows the orbit parameters of the fundamental mode as function of the wavevector and along each sublayer of the reciprocal NiFe layer (Fig. 6(a)-(c)), and the nonreciprocal GML (Fig. 6(d)-(f)) and MD (Fig. 6(g)-(i)) systems. Notice that the tilting angle has only two possible values $\varphi_n^0 = 0, \pi/2$ and the transition between them coincides with the boundary of zero eccentricity. In all our results, zero eccentricity defines the transition point where the larger and smaller semiaxis permute between them, which is therefore consistent with boundary in the tilting angle φ_n^0 that separates the region with $\varphi_n = 0$ (larger semiaxis along \hat{x}_n) from the region with $\varphi_n^0 = \pi/2$ (larger semiaxis along \hat{y}_n). One can also observe that the phase shift angle takes only discrete angles $\tau_n = \pm l\pi/2$ with $l = 0, 1, 2, \dots$, with well-defined boundaries between them. The addition $\tilde{\tau}_n = \varphi_n^0 + \tau_n$ defines the orientation of the dynamic magnetization at zero time $\mathbf{m}_n[t = 0]$. Fig. 5 shows the possible orientations of the $\mathbf{m}_n[t = 0]$ accord-

ing to the addition of the possible values of φ_n^0 and τ_n , and is very useful to understand the SW orbit distribution along the thickness shown at the two rightmost column of Fig. 6 at $\pm k_x = 20 \text{ rads}/\mu\text{m}$. Here, the blue-circle and empty blue-circle points correspond to $\mathbf{m}_n[t = 0]$ and $\mathbf{m}_n[t = \pi/2]$, respectively. Notice the inversion symmetry of the orbit parameters (i.e., $\epsilon_n[k_x] = \epsilon_{N-n}[-k_x]$, $\varphi_n^0[k_x] = \varphi_{N-n}^0[-k_x]$, and $\tau_n[k_x] = \tau_{N-n}[-k_x]$) which is consistent with the SW mode heterosymmetry of the reciprocal NiFe homogeneous layer (see Figs. 6(a)-(c)). In contrast, the lack of inversion symmetry of the orbit parameters in the nonreciprocal MD and GML systems (as shown in Figs. 6(d)-(h)) is consistent with that the counterpropagating SW modes at the same wavevector magnitude k_x are no more heterosymmetric. According to this, one could say that Fig. 6 gives a widespread overview of the mode heterosymmetry at a given range of wavevectors, therefore, useful to get an idea on how nonreciprocal the system is.

According to Eqs. (33)-(36) and noticing that the orbit parameters differences between two counterpropagating SW modes at the same wavevector magnitude k_x are such that $\Delta\phi_n^0 = 0, \pm\pi/2, \pm\pi$ and $\Delta\tau_n = \pm l\pi/2$ with $l = 0, 1, 2, \dots$, thus the entries of the $N \times N$ diagonal matrices \mathbb{R}_{11} and \mathbb{R}_{12} are real or pure imaginary numbers. As mentioned in previous sections, \mathbb{R}_{11} and \mathbb{R}_{12} are mutually exclusive real or pure imaginary matrices (i.e., if \mathbb{R}_{11} is real (pure imaginary), thus \mathbb{R}_{12} is pure imaginary (real)). At the fundamental counterpropagating order mode, \mathbb{R}_{11} and \mathbb{R}_{12} turns out to be real and pure imaginary matrices, respectively (see supplementary material for \mathbb{R}_{11} and \mathbb{R}_{12} values at higher counterpropagating order modes). In Fig. 7, we show these matrices for the fundamental order mode of the reciprocal homogeneous NiFe layer with homogeneous magnetization pointing along \hat{z} (see Fig. 7(a) and (d)), the MD system (see Fig. 7(b) and (e)) and GML system (see Fig. 7(c) and (f)).

In the case of the reciprocal homogeneous NiFe layer with homogeneous magnetization, the inversion symmetry of the orbit parameters is consistent with the even symmetry $R_{11}^n = R_{11}^{N-n}$ and the odd symmetry $R_{12}^n = -R_{12}^{N-n}$ along the thickness of the magnetic layer, as seen in Fig. 7(a), (d), (g), and (j) for the fundamental SW order mode. The same symmetries apply to higher SW order modes in the reciprocal layer (see supplementary material). These results helps to contrast with the nonreciprocal MD and GML systems, featured by the lack of inversion symmetry in their orbit parameters, which is consistent with the lack of even or odd symmetries in the same matrix entries. This lack of symmetry can be considered as a signature of a nonreciprocal dispersion relation dominated mostly by the interlayer exchange interaction.

The lack of inversion symmetry of \mathbb{R}_{11} and \mathbb{R}_{12} also has consequences in the matrix structure of the FSDM, \mathbb{W} , via eqs. (23)-(26). Nevertheless, an discussion about its matrix structure is led to a next manuscript, since including it here would be redundant.

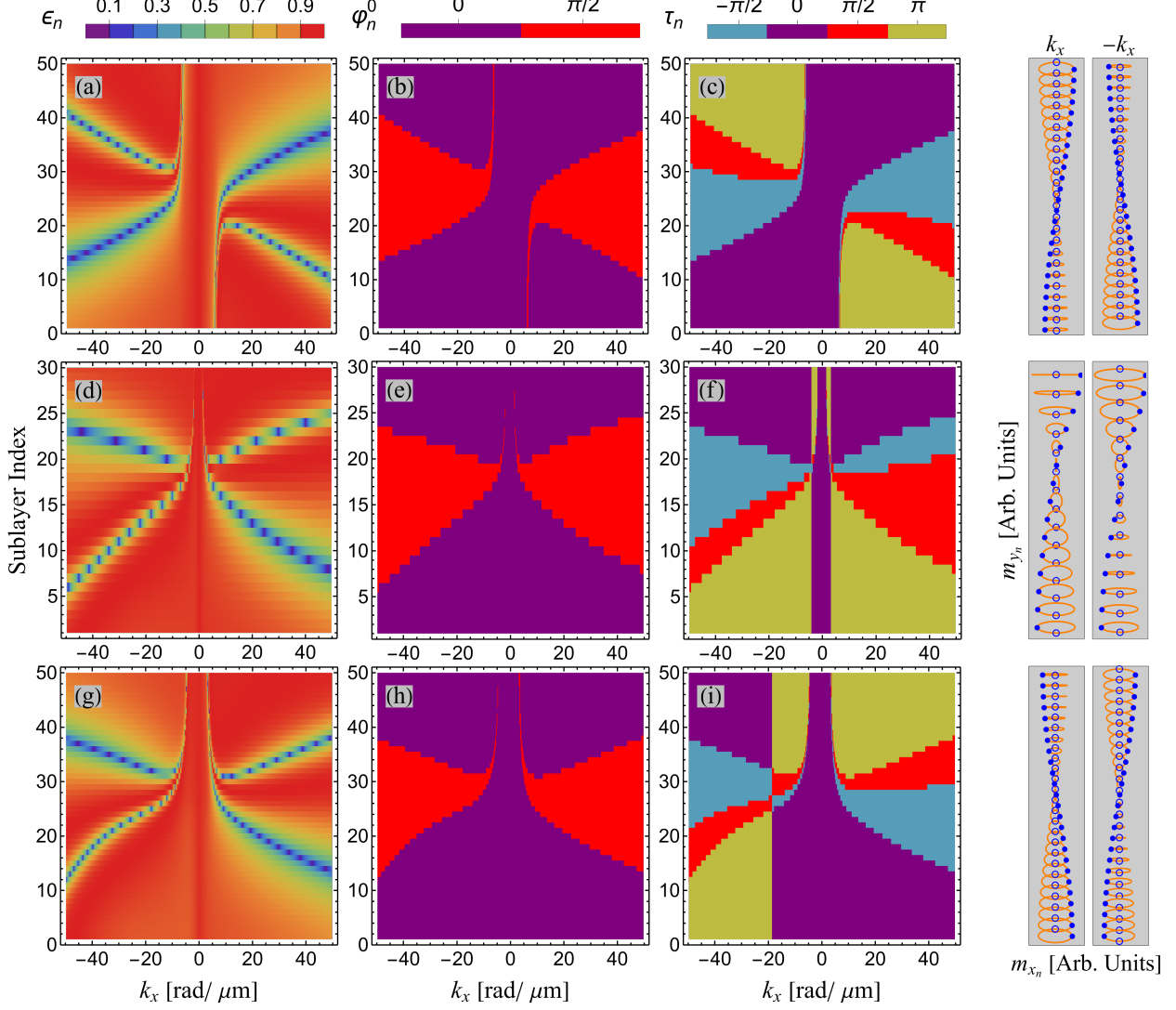


Figure 6. Spin wave orbit parameters distribution along the system thickness as function of the wavevector k_x . Eccentricity ϵ_n , tilting angle φ_n^0 and phase shift angle τ_n are shown for three different multilayered systems with in-plane homogeneous magnetization parallel to \hat{z} : (a)-(c) a single layer of NiFe with saturation magnetization, stiffness constant, thickness and uniaxial anisotropy given as $M_s^{\text{NiFe}} = 845$ kA/m, $A_{\text{NiFe}} = 12.8$ pJ/m, $d_{t,\text{NiFe}} = 50$ nm, and $K_{\text{NiFe}} = 0$, respectively; (d)-(f) a planar NiFe layer with graded magnetization saturation along the thickness whose profile changes from $M_s = 800$ kA/m to $M_s = 1600$ kA/m, a thickness $d_{t,\text{NiFe}} = 60$ nm and a stiffness constant $A_{\text{NiFe}} = 11$ pJ/m. For this system, the applied field is $\mu_0 H = 1.5$ mT along the saturation magnetization direction; (g)-(i) a CoFeB/NiFe bilayer with saturation magnetization, stiffness constant, thickness and uniaxial anisotropy constant as $M_s^{\text{CoFeB}} = 1270$ kA/m ($M_s^{\text{NiFe}} = 845$ kA/m), $A_{\text{CoFeB}} = 17$ pJ/m ($A_{\text{NiFe}} = 12.8$ pJ/m), $d_{t,\text{CoFeB}} = 25$ nm ($d_{t,\text{NiFe}} = 25$ nm) and $K_{\text{CoFeB}} = 0$ ($K_{\text{NiFe}} = 0$), respectively, with an applied magnetic field $\mu_0 H = 30$ mT.

IV. CONCLUSIONS

We have presented a unified theoretical framework to identify the microscopic origin of spin-wave nonreciprocity in planar multilayer magnetic heterostructures without Dzyaloshinskii-Moriya interaction. Using a frequency-shift dynamic matrix together with an interaction-resolved dy-

namic energy-density analysis, we showed that the dispersion asymmetry generally cannot be attributed solely to dipolar interactions. Instead, once counter-propagating modes differ in their geometric structure along the thickness - a generic situation in multilayer systems beyond the thin-film limit - the frequency shift is dominated by exchange interactions, with the regular isotropic exchange along the film thickness (re-

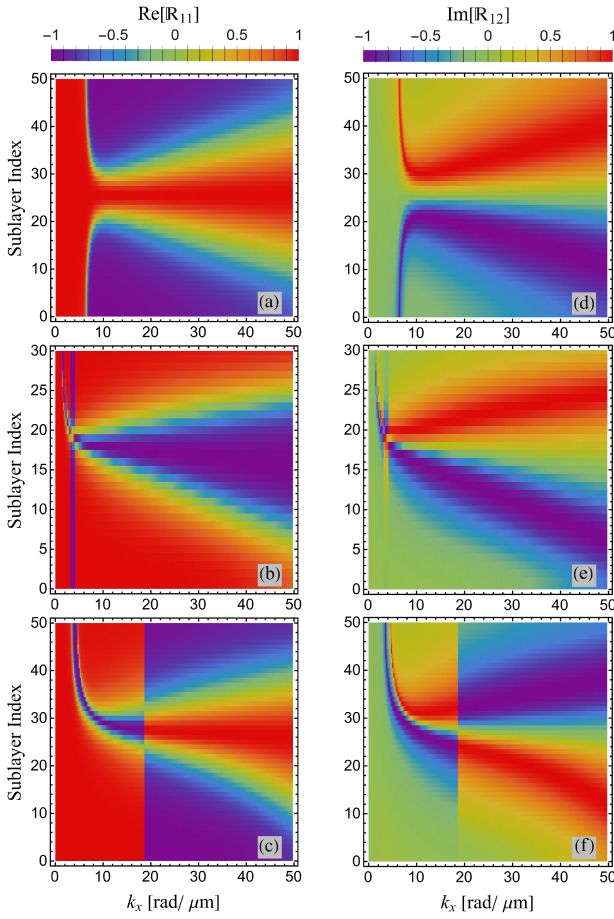


Figure 7. $N \times N$ diagonal matrices profile along the system thickness and as function of the wavevector magnitude k_x for the fundamental SW order mode in a Damon-Esbach configuration and homogeneous magnetization. (a)-(c) and (d)-(f) show the profile of $\mathbb{R}_{11} = \text{Re}[\mathbb{R}_{11}]$ and $\mathbb{R}_{12} = \text{Im}[\mathbb{R}_{12}]$, respectively. Matrices comparison among three systems: (a) and (d) for a reciprocal and homogeneous single NiFe layer, with saturation magnetization, stiffness constant, thickness and uniaxial anisotropy given as $M_s^{\text{NiFe}} = 845 \text{ kA/m}$, $A_{\text{NiFe}} = 12.8 \text{ pJ/m}$, $d_{t,\text{NiFe}} = 50 \text{ nm}$, and $K_{\text{NiFe}} = 0$, respectively; (b) and (e) corresponding to a planar NiFe layer with graded magnetization saturation along the thickness whose profile changes from $M_s = 800 \text{ kA/m}$ to $M_s = 1600 \text{ kA/m}$, a thickness $d_{t,\text{NiFe}} = 60 \text{ nm}$ and a stiffness constant $A_{\text{NiFe}} = 11 \text{ pJ/m}$. For this system, the applied field is $\mu_0 H = 1.5 \text{ mT}$ along the saturation magnetization direction; and (c) and (f) corresponding to a CoFeB/NiFe bilayer with saturation magnetization, stiffness constant, thickness and uniaxial anisotropy constant as $M_s^{\text{CoFeB}} = 1270 \text{ kA/m}$ ($M_s^{\text{NiFe}} = 845 \text{ kA/m}$), $A_{\text{CoFeB}} = 17 \text{ pJ/m}$ ($A_{\text{NiFe}} = 12.8 \text{ pJ/m}$), $d_{t,\text{CoFeB}} = 25 \text{ nm}$ ($d_{t,\text{NiFe}} = 25 \text{ nm}$) and $K_{\text{CoFeB}} = 0 \text{ kJ/m}^3$ ($K_{\text{NiFe}} = 0$), respectively, with an applied magnetic field $\mu_0 H = 30 \text{ mT}$.

ferred to as interlayer exchange throughout the manuscript) providing the leading contribution.

Purely dipolar nonreciprocity emerges only in the special case where the normalized spin-wave profiles at $\pm k$ are identical layer by layer. In all other cases, the dominant contribution to the frequency shift originates from the imbalance

of exchange-mediated energy by counter-propagating modes. By evaluating realistic parameter ranges and analyzing two representative systems - a graded-magnetization NiFe film and a CoFeB/NiFe bilayer - we demonstrated that the interlayer exchange contribution exceeds the dipolar and intralayer exchange contributions by up to two to three orders of magnitude over a broad wave-vector range.

Finally, we examined the symmetry properties of spin-wave orbits through their eccentricity ϵ_n , tilt angle φ_n^0 , and phase shift τ_n . For a homogeneous NiFe layer with reciprocal dispersion, these orbit parameters exhibit inversion symmetry, consistent with the heterosymmetric nature of the counter-propagating modes. In contrast, both the magnonic diode and graded-magnetization systems display nonreciprocal dispersion and nonheterosymmetric mode profiles, leading to broken inversion symmetry in the orbit parameters. These symmetry differences are directly reflected in the structure of the matrices \mathbb{R}_{11} and \mathbb{R}_{12} , which exhibit even and odd thickness symmetries, respectively, in the homogeneous case, and lack such symmetries in the nonreciprocal systems.

Physically, dipolar interactions generate asymmetric mode profiles, while the energetic cost of this asymmetry is set primarily by interlayer exchange, which strongly penalizes profile inhomogeneity. Expressing the frequency-shift dynamic matrix in terms of orbit geometry parameters clarifies how these geometric differences are converted into large frequency shifts. Our results revise the common interpretation of nonreciprocal spin-wave dispersion in multilayers and establish isotropic exchange as the leading interaction responsible for nonreciprocity. With this, we provide fundamental physical insight with direct implications for the design and optimization of multilayer magnonic devices, such as diodes, isolators, and directional wave-based computing architectures, which might encourage further developments in the emerging field of 3D magnon devices for improving the capabilities of transferring, buffering and processing information.

DECLARATION OF COMPETING INTEREST

The authors declare that they have no known competing financial interests or personal relationships that could have appeared to influence the work reported in this paper.

ACKNOWLEDGMENTS

This research has received funding support from Chilean Doctorado Nacional ANID via fellowship Grant 21211429.

DATA AVAILABILITY STATEMENT

The data that support the findings of this study are available within the article [and its supplementary material]

CREDIT AUTHORSHIP CONTRIBUTION STATEMENT

Claudia Negrete: Writing - original draft, Visualization, Conceptualization, Investigation, Formal Analysis. **Attila Kákay:** Writing - review & editing, Conceptualization, Investigation. **Jorge A. Otálora:** Writing - review & editing, Conceptualization, Supervision, Resources, Project administration, Methodology, Investigation, Formal Analysis.

REFERENCES

- ¹A. V. Chumak, V. I. Vasyuchka, A. A. Serga, and B. Hillebrands, *Nature Physics* **11**, 453 (2015).
- ²K. L. Wong, L. Bi, M. Bao, Q. Wen, J. P. Chatelon, Y.-T. Lin, C. A. Ross, H. Zhang, and K. L. Wang, *Applied Physics Letters* **105**, 232403 (2014).
- ³J. Chen, H. Yu, and G. Gubbiotti, *Journal of Physics D: Applied Physics* **55**, 123001 (2021).
- ⁴R. Camley, *Surface Science Reports* **7**, 103 (1987).
- ⁵A. Savchenko and V. Krivoruchko, *Journal of Magnetism and Magnetic Materials* **474**, 9 (2019).
- ⁶A. V. Chumak, P. Kabos, M. Wu, C. Abert, C. Adelmann, A. O. Adeyeye, J. Åkerman, F. G. Aliev, A. Anane, A. Awad, C. H. Back, A. Barman, G. E. W. Bauer, M. Becherer, E. N. Beginin, V. A. S. V. Bittencourt, Y. M. Blanter, P. Bortolotti, I. Boventer, D. A. Bozhko, S. A. Bunyaev, J. J. Carmiggelt, R. R. Cheenikundil, F. Ciubotaru, S. Cotofana, G. Csaba, O. V. Dobrovolskiy, C. Dubs, M. Elyasi, K. G. Fripp, H. Fulara, I. A. Golovchanskiy, C. Gonzalez-Ballester, P. Graczyk, D. Grundler, P. Gruszecki, G. Gubbiotti, K. Guslienko, A. Haldar, S. Hamdioui, R. Hertel, B. Hillebrands, T. Hioki, A. Houshang, C.-M. Hu, H. Huebl, M. Huth, E. Iacocca, M. B. Jungfleisch, G. N. Kakazei, A. Khitun, R. Khymin, T. Kikkawa, M. Kläui, O. Klein, J. W. Klos, S. Knauer, S. Koraltan, M. Kostylev, M. Krawczyk, I. N. Krivorotov, V. V. Kruglyak, D. Lachance-Quirion, S. Ladak, R. Lebrun, Y. Li, M. Lindner, R. Macêdo, S. Mayr, G. A. Melkov, S. Miesczak, Y. Nakamura, H. T. Nembach, A. A. Nikitin, S. A. Nikitov, V. Novosad, J. A. Otálora, Y. Otani, A. Papp, B. Pigeau, P. Pirro, W. Porod, F. Porrati, H. Qin, B. Rana, T. Reimann, F. Riente, O. Romero-Isart, A. Ross, A. V. Sadovnikov, A. R. Safin, E. Saitoh, G. Schmidt, H. Schultheiss, K. Schultheiss, A. A. Serga, S. Sharma, J. M. Shaw, D. Suess, O. Surzhenko, K. Szulc, T. Taniguchi, M. Urbánek, K. Usami, A. B. Ustinov, T. van der Sar, S. van Dijken, V. I. Vasyuchka, R. Verba, S. V. Kusminskiy, Q. Wang, M. Weides, M. Weiler, S. Wintz, S. P. Wolski, and X. Zhang, *IEEE Transactions on Magnetics* **58**, 1 (2022).
- ⁷F. Ma and Y. Zhou, *RSC Adv.* **4** (2014).
- ⁸Q. Wang, A. V. Chumak, and P. Pirro, *Nature Communications* **12**, 2636 (2021).
- ⁹N. Zenbaa, K. O. Levchenko, J. Panda, K. Davídková, M. Ruhwedel, S. Knauer, M. Lindner, C. Dubs, Q. Wang, M. Urbánek, P. Pirro, and A. V. Chumak, *IEEE Magnetics Letters* **16**, 1 (2025).
- ¹⁰M. Jamali, J. H. Kwon, S.-M. Seo, K.-J. Lee, and H. Yang, *Scientific Reports* **3**, 3160 (2013).
- ¹¹A. Khitun, M. Bao, and K. L. Wang, *Journal of Physics D: Applied Physics* **43**, 264005 (2010).
- ¹²A. Khitun and A. Kozhanov, *Magnonic logic devices*, in *Nanomagnetic and Spintronic Devices for Energy-Efficient Memory and Computing* (Wiley, 2015) pp. 189–219.
- ¹³I. Harward, R. Camley, and Z. Celinski, *Applied Physics Letters* **105** (2014).
- ¹⁴A. F. Franco, *New Journal of Physics* **22** (2020).
- ¹⁵M. Grassi, M. Geilen, D. Louis, M. Mohseni, T. Brächer, M. Hehn, D. Stoeffler, M. Bailleul, P. Pirro, and Y. Henry, *Phys. Rev. Appl.* **14**, 024047 (2020).
- ¹⁶J. Zou, S. Bosco, E. Thingstad, J. Klinovaja, and D. Loss, *Phys. Rev. Lett.* **132**, 036701 (2024).
- ¹⁷L. Körber, R. Verba, J. A. Otálora, V. Kravchuk, J. Lindner, J. Fassbender, and A. Kákay, *Phys. Rev. B* **106**, 014405 (2022).
- ¹⁸J. A. Otálora, M. Yan, H. Schultheiss, R. Hertel, and A. Kákay, *Phys. Rev. B* **95**, 184415 (2017).
- ¹⁹M. Salazar-Cardona, L. Körber, H. Schultheiss, K. Lenz, A. Thomas, K. Nielsch, A. Kákay, and J. Otálora Arias, *Applied Physics Letters* **118**, 262411 (2021).
- ²⁰R. Gallardo, P. Alvarado-Seguel, and P. Landeros, *Phys. Rev. Appl.* **18**, 054044 (2022).
- ²¹V. Sluka, T. Schneider, R. A. Gallardo, A. Kákay, M. Weigand, T. Wintz, R. Mattheis, A. Roldán-Molina, P. Landeros, V. Tiberkevich, A. Slavin, G. Schütz, A. Erbe, A. Deac, J. Lindner, J. Raabe, J. Fassbender, and S. Wintz, *Nature Nanotechnology* **14**, 328–333 (2019).
- ²²R. A. Gallardo, P. Alvarado-Seguel, T. Schneider, C. Gonzalez-Fuentes, A. Roldán-Molina, K. Lenz, J. Lindner, and P. Landeros, *New Journal of Physics* **21**, 033026 (2019).
- ²³L. Christienne, J. Jiménez-Bustamante, P. Rovillain, M. Eddrief, Y. Zheng, F. Fortuna, M. Marangolo, M. Madami, R. Gallardo, P. Landeros, and S. Tacchi, arXiv:2504.11145 [cond-mat] 10.48550/arXiv.2504.11145 (2025), arXiv:2504.11145 [cond-mat].
- ²⁴B. Mimica-Figari, P. Landeros, and R. Gallardo, arXiv:2504.12219 [cond-mat] 10.48550/arXiv.2504.12219 (2025), arXiv:2504.12219 [cond-mat].
- ²⁵K. Zakeri, Y. Zhang, J. Prokop, T.-H. Chuang, N. Sakr, W. X. Tang, and J. Kirschner, *Phys. Rev. Lett.* **104**, 137203 (2010).
- ²⁶M. Kuepferling, A. Casiraghi, G. Soares, G. Durin, F. Garcia-Sánchez, L. Chen, C. H. Back, C. H. Marrows, S. Tacchi, and G. Carlotti, *Rev. Mod. Phys.* **95**, 015003 (2023).
- ²⁷C. Heins, V. Iurchuk, O. Gladii, L. Körber, A. Kákay, J. Fassbender, K. Schultheiss, and H. Schultheiss, *Phys. Rev. B* **111**, 134434 (2025).
- ²⁸M. Huang, Y. Liu, W. Hu, Y. Wu, W. Wang, W. He, H. Zhang, and F. Bai, *Phys. Rev. Appl.* **21**, 014035 (2024).
- ²⁹S.-W. Cheong, D. Talbayev, V. Kiryukhin, and A. Saxena, *npj Quantum Materials* **3**, 19 (2018).
- ³⁰S.-W. Cheong and X. Xu, *npj Quantum Materials* **7**, 40 (2022).
- ³¹L. Körber, *Spin Waves in Curved Magnetic Shells*, Ph.D. thesis, Technische Universität Dresden, Dresden (2023), helmholtz-Zentrum Dresden-Rossendorf. Supervisors: Dr. rer. nat. Attila Kákay and Prof. Dr. rer. nat. Jürgen Fassbender.
- ³²R. Claes and K. Meerbergen, *Applied Mathematics Letters* **135**, 108412 (2023).
- ³³P. Xiao-Feng and F. Yuan-Ping, *Quantum Mechanics in Nonlinear Systems* (WORLD SCIENTIFIC, 2005) <https://www.worldscientific.com/doi/pdf/10.1142/5721>.
- ³⁴Y. Henry, O. Gladii, and M. Bailleul, arXiv:1611.06153 [cond-mat] (2016), comment: 23 pages, 16 figures, arXiv:1611.06153 [cond-mat].